

1 **This pre-print is currently under review at SCIENTIFIC DATA and has been peer reviewed**
2 **and approved for publication consistent with U.S. Geological Survey Fundamental**
3 **Science Practices (pubs.usgs.gov/circ/1367/).**

4 National-scale, remotely sensed lake trophic state, 1984-2020

5
6 Michael F Meyer^{1,2,*}, Simon N Topp³, Tyler V King⁴, Robert Ladwig², Rachel M Pilla⁵,
7 Hilary A Dugan², Jack R Eggleston⁶, Stephanie E Hampton⁷, Dina M Leech⁸, Isabella A
8 Oleksy⁹, Jesse C Ross¹⁰, Matthew RV Ross¹¹, R Iestyn Woolway¹², Xiao Yang¹³,
9 Matthew R Brousil¹¹, Kate C Fickas^{14,15}, Julie C Padowski¹⁶, Amina I Pollard¹⁷, Jianning
10 Ren¹⁸, Jacob A Zwart¹⁹

11

12 ¹ U.S. Geological Survey, Madison, WI, USA

13 ² University of Wisconsin - Madison, Madison, WI, USA

14 ³ U.S. Geological Survey, Carrboro, NC, USA

15 ⁴ U.S. Geological Survey, Boise, ID, USA

16 ⁵ Oak Ridge National Laboratory, Oak Ridge, TN, USA

17 ⁶ U.S. Geological Survey, Kearneysville, WV, USA

18 ⁷ Carnegie Institution for Science, Pasadena, CA, USA

19 ⁸ Longwood University, Farmville, VA, USA

20 ⁹ University of Wyoming, Laramie, WY, USA

21 ¹⁰ U.S. Geological Survey, Los Angeles, CA, USA

22 ¹¹ Colorado State University, Fort Collins, CO, USA

23 ¹² Bangor University, Menai Bridge, Anglesey, UK

24 ¹³ Southern Methodist University, Dallas, TX, USA

25 ¹⁴ U.S. Geological Survey, Sioux Falls, SD, USA

26 ¹⁵ University of California - Santa Barbara, Santa Barbara, CA, USA

27 ¹⁶ Washington State University, Pullman, WA, USA

28 ¹⁷ U.S. Environmental Protection Agency, Washington DC, USA

29 ¹⁸ University of Nevada - Reno, Reno, NV, USA

30 ¹⁹ U.S. Geological Survey, Pittsburgh, PA, USA

31

32 *Corresponding Author: mfmeyer@usgs.gov

33

34

35 **Abstract (155 of 170 words)**

36

37 Lake trophic state is a key ecosystem property that integrates a lake's physical,
38 chemical, and biological processes. Despite the importance of trophic state as a gauge
39 of lake water quality, standardized and machine-readable observations are uncommon.
40 Remote sensing presents an opportunity to detect and analyze lake trophic state with
41 reproducible, robust methods across time and space. We used Landsat surface
42 reflectance data to create the first compendium of annual lake trophic state for 55,662
43 lakes of at least 10 ha in size throughout the contiguous United States from 1984
44 through 2020. The dataset was constructed with FAIR data principles (Findable,
45 Accessible, Interoperable, and Reproducible) in mind, where data are publicly available,
46 relational keys from parent datasets are retained, and all data wrangling and modeling
47 routines are scripted for future reuse. Together, this resource offers critical data to
48 address basic and applied research questions about lake water quality at a suite of
49 spatial and temporal scales.

50

51 **Background and Summary**

52

53 Lakes and reservoirs are of critical importance to society, directly providing drinking
54 water and supporting food production, sanitation, and transportation. Millions of people
55 worldwide face intermittent clean water availability due to climatic and anthropogenic
56 stressors¹. Current literature suggests that changes in surface water quantity and
57 quality are highly heterogeneous, and trends globally suggest that factors such as ice
58 cover, air temperature, humidity, and lake surface area are likely interacting regionally
59 to affect freshwater ecosystems in synergistic ways²⁻⁷. To gain a better understanding
60 of the potential threats to freshwater ecosystems, new technologies must be engaged.
61 Satellite-based Earth observations (hereafter "remote sensing") are particularly useful
62 as they can provide information at spatial and temporal scales that are currently
63 impossible to replicate via ground-based observations.

64

65 Although remote sensing's usefulness to track changes in water quantity has enabled
66 analyses of water availability from local-to-global scales⁸⁻¹¹, investigations of water
67 quality have historically been more limited in scale and scope. However, remote sensing
68 now offers powerful approaches to assessing patterns and trends in water quality^{2,12-15},
69 and data harmonization efforts allow for greater interoperability between *in situ*
70 collections and remote sensing imagery^{16,17}. Among studies of remotely sensed metrics
71 of water quality, the majority have centered around specific constituents, such as
72 chlorophyll or suspended sediment, without necessarily offering holistic metrics of
73 ecosystem integrity.

74

75 Lake trophic state (LTS) is an example of a metric intended to provide holistic
76 assessments of a lake's aggregate physical (e.g., light attenuation), chemical (e.g.,
77 nutrient concentrations), and biological processes (e.g., productivity). Within the
78 limnological community, LTS is a property closely associated with a lake's characteristic
79 autochthonous and allochthonous productivity as well as water color. Broadly speaking,
80 eutrophic lakes are green, oligotrophic lakes are blue, and dystrophic lakes are brown

81 (Figure 1). From color-trophic state connections, fundamental limnological principles
82 center around linking trophic states to characteristic properties (Figure 1). For example,
83 oligotrophic lakes are usually characterized by having lower phosphorus concentrations,
84 low offshore but comparably higher nearshore productivity, and low colored dissolved
85 organic matter (Figure 1). In contrast, eutrophic lakes have higher phosphorus
86 concentrations and higher phytoplankton biomass (Figure 1).

87
88 In a management context, the language of LTS has historically been used to describe
89 conditions relative to nutrient enrichment. For example, following the 1971
90 announcement of US Federal efforts to limit the use of phosphorus in detergents, the
91 U.S. Environmental Protection Agency (U.S. EPA) and state water resource
92 management agencies launched a National Eutrophication Survey¹⁸. The survey
93 assessed trophic state, defined as nutrient enrichment, of lakes influenced by
94 wastewater treatment plants. In this case, LTS language was used to focus on and
95 communicate about eutrophication, whereas dystrophication aspects of the framework
96 were not as prominent. These language patterns likely carry over to contemporary uses.
97 Because discussions may have focused on eutrophication in the past, modern tools and
98 frameworks could be enhanced by remotely sensed water quality data that capture
99 aspects of both eutrophication and dystrophication. For example, as climate changes,
100 drinking water utility managers will increasingly face compounding hazards that could
101 negatively impact lakes and reservoirs that supply hundreds of millions of people with
102 drinking water¹⁹. Data and tools that provide remotely sensed information on LTS could
103 improve the ability to observe multidecadal changes in water quality and save resources
104 by better targeting field monitoring.

105
106 Although LTS is often employed as a classification system for characterizing autotrophic
107 production²⁰, the Nutrient-Color Paradigm (NCP) is an empirically tested framework for
108 discriminating LTS based off two variables: (1) phosphorus concentrations, a proxy for
109 primary productivity; and (2) colored dissolved organic matter or turbidity measured in
110 platinum-cobalt units, both proxies for water transparency^{21–23}. By combining
111 characteristic metrics of a lake's primary productivity and optical properties, the NCP
112 presents a powerful system for discriminating LTS, where both autochthonous and
113 allochthonous processes are considered. Leveraging the relationship between LTS,
114 phosphorus concentrations, and water clarity, it is possible to transform remotely
115 sensed lake surface reflectance observations into meaningful limnological and
116 ecosystem properties.

117
118 Here, we present the first national-scale compendium of LTS that has been built from
119 remotely sensed lake color (i.e., spectral signatures). The dataset, referred to as LTS-
120 US, is derived from (1) coordinated, continental-scale *in situ* measurements, where LTS
121 has been documented for select lakes and years, and (2) characteristic Landsat surface
122 reflectance values for each lake's Chebyshev center (the point in a polygon furthest
123 from the edge). Using *in situ* LTS, we can build predictive models to associate LTS with
124 characteristic reflectance values, and then apply predictive models to lakes with
125 unknown trophic states. Together, the dataset contains predictions for 55,662 lakes of
126 at least 10 ha in area with annual estimates of LTS from 1984 through 2020. By

127 coupling satellite-based remote sensing with fundamental limnological principles, the
128 LTS-US dataset provides the means to apply the NCP at the national scale to identify
129 macroscale patterns and trends in LTS. Further, this approach moves beyond remote
130 sensing of individual parameters to provide insights into lakes' physical, chemical,
131 biological, and ecosystem properties.

132

133 **Methods**

134

135 The LTS-US dataset is constructed using a four-part pipeline, as shown in Figure 2: (1)
136 aggregate training data, (2) create classification models, (3) apply predictions to lakes
137 outside of the training data, and (4) assess model performance and prediction validity.
138 Individual steps within the pipeline are described below.

139

140 Step 1: Identify Parent Datasets

141

142 *U.S. Environmental Protection Agency National Lakes Assessment*

143

144 *In situ* measurements of total phosphorus and true color were compiled from the U.S.
145 EPA's National Lakes Assessment (NLA)^{24–28}, a synoptic sampling campaign of lakes,
146 ponds, and reservoirs, hereafter collectively referred to as “lakes”, conducted in the
147 contiguous U.S. every five years. Lakes used in this analysis were sampled in the
148 summer (June–September) of 2007 (n = 1,028), 2012 (n = 1,038), or 2017 (n = 1,005).
149 Lakes were selected from the National Hydrography Dataset (NHD,
150 <https://www.usgs.gov/national-hydrography/national-hydrography-dataset>) using a
151 randomized design stratified on aggregated Omernik level III ecoregion²⁹ and lake
152 surface area. The minimum surface area for inclusion in the 2007 assessment was 4
153 ha, but, owing to increasing resolution in the NHD, was reduced to 1 ha for the 2012
154 and 2017 assessments. Natural lakes and reservoirs were treated equally in the site
155 selection process.

156

157 To inform internal quality assurance within a campaign, 10% of the lakes were sampled
158 twice within a field season. Approximately 25% of lakes were targeted for resampling in
159 multiple years to examine temporal change. State, Tribal, Federal, and contractor field
160 crews evaluated lakes on site to ensure that selected lakes met criteria for inclusion in
161 the field campaign (e.g., lake ≥ 1 m deep). A wide set of measurements were collected
162 at each sampled lake, but we only provide details on the variables used in this analysis.
163 Additional details, protocols, and data are available online
164 (<https://www.epa.gov/national-aquatic-resource-surveys/nla>).

165

166 Total phosphorus and true color were collected and processed in the 2007, 2012, and
167 2017 field campaigns^{24–26}. Water samples were collected from a deep (up to 50 m),
168 open water location in natural lakes and at a midpoint in reservoirs. In natural lakes,
169 field crews were asked to sample in a deep area of the lake regardless of whether the
170 sample location was in the geometric center of the system. In reservoirs, field crews
171 were asked to try to find a midpoint in the system that is reasonably lentic, deep (up to
172 50 m), and away from the dam. Water was collected from the photic zone using a

173 vertical, depth integrated sampling device. All water samples were placed on ice and
174 shipped overnight to the Willamette Research Station in Corvallis, Oregon for analysis.
175 True color was estimated by visual comparison of filtered water samples to a calibrated
176 glass color disk³⁰. Total phosphorus concentrations were measured with manual
177 alkaline persulfate digestion, followed by automated colorimetric analysis (ammonium
178 molybdate and antimony potassium tartrate under acidic conditions, with absorbance at
179 880 nm) using a flow injection analyzer following standard method 4500-P-E³¹. Detailed
180 descriptions of all water quality analyses are available in the NLA Laboratory Operations
181 Manuals^{24,27,28}.

182 183 *HydroLAKES*

184
185 HydroLAKES (v1.0)³² is a compendium of more than 1.4 million lake and reservoir
186 shapefiles globally, with surface area of at least 10 ha. For an individual waterbody,
187 HydroLAKES contains its spatial extent and location (using georeferenced polygons), a
188 unique identifier (ranging from 1 to 1,427,688), and its morphological (area, mean
189 depth, elevation, shoreline length etc.), hydrological (e.g., residence time, discharge,
190 and watershed area), and geographical (e.g., name, country, continent) properties.
191 HydroLAKES is a compilation of existing lake databases, with sources from government
192 agencies (e.g., Natural Resources Canada, U.S. Geological Survey, European
193 Environment Agency) and from remote sensing studies (for example, Shuttle Radar
194 Topographic Mission Water Body Data, Global Lakes and Wetlands Database, and
195 Global Reservoir and Dam Database). Most of the lake polygons are sourced from the
196 Shuttle Radar Topographic Mission Water Body Data for regions between 60°S and
197 60°N³³, supplemented by other datasets for higher latitudes and for underrepresented
198 regions. More detailed information on the creation and validation of the HydroLAKES
199 dataset can be found in Messenger et al.³².

200 201 *LimnoSat*

202
203 The LimnoSat-US³⁴ dataset comprises over 22 million remotely sensed observations of
204 lake surface reflectance from 1984 to 2020. Observations cover 55,662 lakes greater
205 than 10 ha³² aggregated from Landsat 5, 7, and 8 Collection 1 imagery. Each
206 observation was calculated by taking the median surface reflectance within 120 meters
207 of each lake's Chebyshev center, defined as the point farthest from shore and usually
208 located at the lake's deepest point³⁵. Extracting reflectance values from the Chebyshev
209 center minimizes signals due to bottom reflectance and adjacent land pixels. For each
210 Landsat observation, non-high confidence water pixels were masked using the Dynamic
211 Surface Water Extent algorithm³⁶. Observations were removed if the scene cloud cover
212 was greater than 75%, any snow, ice, cloud, cloud shadow³⁷, or hillshadow was
213 detected over the lake's Chebyshev center, or if there were fewer than eight high
214 confidence water pixels within the 120 meter buffer of the lake's Chebyshev center. For
215 certain lakes, these filters lead to extended periods (i.e., months to years) with limited
216 observations (see Figure 2 in Topp et al.²). Data in LimnoSat-US are presented in a
217 tabular format, where each row reflects a Landsat overpass for a given waterbody, and
218 columns include median Collection 1 surface reflectance values by band extracted from

219 pixels within 120 m of the Chebyshev center, scene-wide cloud cover, date of imagery
220 acquisition, and number of water pixels within 120 m of the Chebyshev center.

221

222 Step 2: Define Lake Trophic State

223

224 Many lakes across the United States are experiencing simultaneous changes in their
225 water clarity, with some lakes getting greener due to eutrophication, and others getting
226 browner from increasing terrestrially-derived organic matter, and some are
227 simultaneously 'greening' and 'browning'²³. Given the need to discriminate between
228 lakes that may be browning and/or greening, the Nutrient Color Paradigm (NCP) is a
229 useful tool to assign LTS based on a lake's characteristic color.

230

231 The NCP was initially proposed in the early 20th century, emphasizing that both
232 autochthonous and allochthonous processes are important to understanding LTS^{38–40}.
233 Specifically, water color often affects algal biomass and light transparency independent
234 of nutrient availability. Rodhe⁴¹ first assembled the four quadrants of the NCP, placing
235 autochthony on the horizontal axis and allochthony on the vertical axis. This second
236 dimension distinguishes "oligotrophic" (low nutrient, low color) and "eutrophic" (high
237 nutrient, low color) lakes from "dystrophic" (low nutrient, high color) and "mixotrophic"
238 (high nutrient, high color) lakes.

239

240 Although metrics such as Trophic State Index²⁰ gained popularity for providing
241 instantaneous assessments of a lake's autotrophic production, Williamson et al.²¹
242 encouraged a focus on NCP for lake classification given the importance of both
243 nutrients and colored dissolved organic matter to lake structure and function. The NCP's
244 implementation is empirically supported by studies like Webster et al.²², where an
245 analysis of ~1,600 temperate lakes in North America demonstrated that within lakes
246 grouped by total phosphorus concentration (i.e., oligotrophic, mesotrophic, or
247 eutrophic), those with 'browner' color (indicative of dissolved organic matter) had higher
248 volumetric chlorophyll-a concentrations and shallower Secchi disk depths. A similar
249 pattern was observed by Nürnberg and Shaw⁴², which analyzed 600 lakes spanning a
250 latitude of 39°S to 82°N.

251

252 Here, we used the thresholds published in Webster et al.²² to classify lakes in the NLA
253 dataset. Lakes were described as oligotrophic or 'blue' if total phosphorus concentration
254 was less than 30 µg/L and true color was less than 20 platinum cobalt units (PCU),
255 eutrophic or 'green' if total phosphorus was greater than 30 µg/L and true color was less
256 than 20 PCU, dystrophic or 'brown' if total phosphorus was less than 30 µg/L and true
257 color greater than 20 PCU, and mixotrophic or 'murky' if total phosphorus was greater
258 than 30 µg/L and true color greater than 20 PCU (Figure 1). Thresholds for total
259 phosphorus are based on long established and widely accepted ranges affecting
260 primary productivity⁴³. True color thresholds are derived from Nürnberg and Shaw⁴².
261 Eutrophic and mixotrophic classifications were combined into a single grouping due to
262 similar spectral characteristics (see Step 3).

263

264 Step 3: Create a training dataset

265
266 First, to create a dataset of lakes with *in situ* LTS measurements, we aggregated all
267 total phosphorus and true color measurements from the U.S. EPA NLA 2007, 2012, and
268 2017 data (Figure S1-2, Table S1). Although the NLA includes lakes smaller than 10 ha,
269 we only used lakes of at least 10 ha in area for consistency with the HydroLAKES
270 database. We then assessed the extent to which seasonal shifts in total phosphorus
271 concentrations and true color values may alter interpretation of trophic state for a given
272 lake using the subset of lakes that were sampled intra-annually. For lakes that were
273 sampled multiple times within a U.S. EPA NLA campaign, we calculated the percentage
274 of lakes that transitioned between trophic states within a single year and found that
275 lakes broadly remained in the same NCP trophic state throughout a given summer
276 (85.1% of lakes). Of the lakes that changed trophic state during a sampling season
277 (14.9%), the majority transitioned from oligotrophic (61.5% of changing lakes; 8.7% of
278 all lakes) or dystrophic (15.4% of changing lakes; 2.2% of all lakes) to
279 eutrophic/mixotrophic. Few lakes transitioned from oligotrophic to dystrophic (15.4% of
280 changing lakes; 2.2% of all lakes), and even fewer transitioned to oligotrophic from
281 either dystrophic (3.9% of changing lakes; 0.5% of all lakes) or eutrophic/mixotrophic
282 (3.9% of changing lakes; 0.5% of all lakes). No lakes transitioned from
283 eutrophic/mixotrophic to dystrophic across all three NLA campaigns. Broadly, lakes
284 transitioned between trophic states when lakes were located near a threshold for trophic
285 state delineation (15-45 µg/L total phosphorus or 11-29 PCU). These results mirror
286 those in Leech et al.²³ and suggest that despite some lakes changing trophic states, the
287 majority of lakes do not transition and those that do transition usually fall along an edge
288 of a NCP-determined trophic state. Thus, for lakes sampled twice in one sampling
289 campaign, we averaged total phosphorus and true color estimates.

290
291 Second, to match the *in situ* trophic states with remotely sensed imagery, we merged
292 the complete 2007, 2012, and 2017 NLA dataset with the LimnoSat-US dataset³⁴,
293 where each NLA lake-year had corresponding Landsat spectral data. Because the NLA
294 is designed to describe lakes' summertime conditions, we filtered LimnoSat-US
295 observances for those only occurring in June, July, and August, which we *a priori*
296 defined as the summertime season for the contiguous U.S.; then, to create a
297 characteristic reflectance for a given lake year, we computed each lake-year's median
298 summertime reflectance for red, blue, green, and near-infrared bands. Because
299 LimnoSat-US compiles reflectance values from Landsat 5, 7, and 8, there are
300 differences in the number of images per lake and year. In particular, images from 1984
301 through 1998 were solely collected from Landsat 5, when lakes averaged 3.04 images
302 per summer (minimum average images: 2.43 images; maximum average images: 3.64
303 images). From 1999 through 2012, summertime imagery was gathered from Landsat 5
304 and 7, when lakes averaged 5.64 images per summer (minimum average images: 3.37
305 images; maximum average images: 6.42 images). From 2013 through 2019,
306 summertime imagery was collected from Landsat 7 and 8, when lakes averaged 5.42
307 images per summer (minimum average images: 4.87 images; maximum average
308 images: 5.87 images).

309

310 Third, to better characterize spectral bands' relative reflectance, we normalized each
311 lake's median summertime reflectance for the red, green, blue, and near-infrared band
312 by the sum of the summertime reflectance values of all four bands. This normalization
313 allowed us to differentiate lakes by trophic state based on their most prominent
314 reflectances. For example, we anticipated that oligotrophic lakes would be dominated by
315 high blue and green reflectances relative to the red and near-infrared bands. In contrast,
316 dystrophic lakes would be dominated by the near-infrared band relative to green and
317 red bands, because dystrophic lakes tend to have exceptionally low primary productivity
318 and elevated dissolved organic matter. When assessing mixotrophic and eutrophic
319 lakes, spectral characteristics were nearly identical, and to be conservative, we
320 combined mixotrophic and eutrophic lakes into one category 'eutrophic/mixotrophic'.
321 These relative reflectances for all three lake trophic states were ultimately intended to
322 discriminate among lakes that were optically similar in the visible spectrum (i.e.,
323 oligotrophic and dystrophic lakes). Notably, the decision to use median summertime
324 relative reflectances differed from previous work² that focused on the dominant
325 wavelength, which is an aggregation of wavelengths detected in the visible spectrum
326 and has been used to discriminate autotrophic production (i.e., blue vs green lakes), but
327 not dystrophic states. Thus, our methods are better suited towards discriminating
328 between oligotrophic and dystrophic lakes, because the dominant wavelength approach
329 would consider both of these lake types to be "blue".

330

331 Step 4: Create Classification Models

332

333 To find an optimal performing classifier for lakes with unknown LTS, we employed three
334 classification methods to predict trophic state: multinomial logistic regression⁴⁴, extreme
335 gradient boosting regression⁴⁵, and a neural network using multilayer perceptrons⁴⁶.
336 Logistic regression is a parametric classification method, whereas gradient boosted
337 regression and multilayer perceptrons are machine learning methods. The methods
338 differ in how they make classifications. Using trophic state as a categorical response
339 variable, logistic regression applies a linear regression of log-odds ratios to model the
340 probability of a given trophic state for each lake. In contrast, gradient boosted
341 regression applies decision trees to iteratively improve its predictions. Multilayer
342 perceptrons apply a type of feedforward artificial neural network in which a
343 backpropagation algorithm is used to subsequently update the individual weights of
344 each neuron unit by comparing modeled predictions to the training data.

345

346 For each modeling method, we used z-scored, relative red, green, blue, and near-
347 infrared reflectances as predictors. Model performance and potential for overfitting were
348 assessed using a 90:10 train:test data split with spatial-holdout cross-validation. Initial
349 hyperparameters for the gradient boosted regression and multilayer perceptron models
350 were tuned by holding out 20% of each trophic class from the training observations to
351 use for validation and conducting a coarse grid-search across the hyperparameter
352 space. For each combination of hyperparameters, models were trained until validation
353 performance did not increase for 20 consecutive epochs using categorical cross entropy
354 as the objective function. During the multilayer perceptron hyperparameter tuning, we
355 iterated through model fits using all combinations of 5, 10, and 20 hidden layers as well

356 as a learning rate of 0.01, 0.001, and 0.0005. Multilayer perceptron hyperparameter
357 tuning metrics were optimal for models with 20 hidden units and a learning rate of
358 0.001. During the gradient boosted regression hyperparameter tuning, we iterated
359 through model fits using all combinations of 2, 3, and 4 maximum tree depths,
360 subsample as well as column samples of 0.5 and 0.8, step sizes of 0.01 and 0.1, as well
361 as a minimum child weight of 1 and 3. Gradient boosted regression hyperparameter
362 tuning metrics were optimal for models with a max depth of 4, subsample of 0.5, column
363 sample of 0.5, step size of 0.01, and minimum child weight of 1. For both multilayer
364 perceptron and gradient boosted regression models, best performing hyperparameter
365 tuning metrics were assessed by having lowest validation loss values.

366
367 These hyperparameters were then used in a spatial cross-validation routine⁴⁷, where a
368 given lake was held out as test data if it was included in the training data. During the
369 spatial cross-validation routine, training data were divided into five folds, such that lakes
370 within each test partition were not present in remaining training partitions (i.e., test
371 metrics represent performance on unseen lakes). Training data within each fold were
372 then partitioned into a 90:10 split with 10% of each trophic class set aside for an inner-
373 loop fold validation. Models within each fold were trained using an early stopping criteria
374 of 20 epochs to avoid overfitting on the training data. This inner-fold validation was
375 additionally used to hypertune the best number of epochs for the final models. Finally,
376 overall error metrics were calculated based on the mean prediction accuracy of the test
377 partitions withheld from the inner-loop training of each fold. All reported metrics are
378 based on the test partitions from the spatial cross-validation routine while final models
379 were trained on the full dataset using the hyperparameters identified from the grid-
380 search and inner-loop validation routines. We applied the final models to make
381 predictions for all 55,662 lakes in the LimnoSat-US dataset.

382 383 Step 5: Assess and Compare Model Performance

384
385 To evaluate the final fitted models, we used test data predictions from the spatial-
386 holdout routine to calculate each model's overall and balanced accuracy, receiver-
387 operator-characteristic (ROC) curves, as well as the area under the curve (AUC) of the
388 ROC curve. Overall accuracy was calculated as the sum of true positives and true
389 negatives divided by the total number of LTS predictions. Balanced accuracy was
390 calculated as the sum of a true positive and true negative results for a single lake
391 trophic state. Whereas overall accuracy can be biased towards more prevalent trophic
392 states (i.e., eutrophic and oligotrophic lakes), balanced accuracy is useful to assess a
393 model's capacity to predict more rare trophic states (i.e., dystrophic lakes). As an
394 additional metric of model performance, we calculated the AUC of each model's ROC
395 curve. The ROC curve visually graphs the relationship between the rate of a correct
396 classification with the rate of a false classification. An AUC of 0.5 indicates a false
397 prediction rate increases 1:1 with the rate of a correct prediction. AUCs greater than 0.5
398 imply a model performing better than random, even when a false positive rate is
399 artificially inflated. Thus, comparing overall and balanced accuracy as well as ROC
400 curves and AUCs allowed us to assess how models performed broadly as well as how
401 robustly models predicted trophic state correctly.

402
403 Beyond model performance, we also evaluated whether model coefficients and variable
404 importance for trophic state discrimination reflected NCP groupings. For increased
405 interpretability across all three models, we employed SHAP (SHapley Additive
406 exPlanation) analysis^{48–50} to better understand individual feature importance and
407 influence in model predictions. SHAP analysis yields insight into the marginal
408 contribution of a given feature (e.g., near-infrared spectra) on model output - in this case
409 trophic state - and helps decode ‘black box’ results. Understanding the relative
410 contribution of individual features in trophic state prediction not only helps explain
411 feature roles in model accuracy and misclassification but also quantitatively connects
412 features, such as remotely sensed data, to the biophysical parameters in which LTS
413 prediction is grounded. SHAP feature contribution was calculated for blue, green, red,
414 and near-infrared Landsat spectra. SHAP feature contribution was scored for
415 oligotrophic, dystrophic, and eutrophic/mixotrophic classifications and across each of
416 the three models. This scoring illuminates the relationship among feature values and
417 SHAP contribution for a given trophic state classification and for a given model.
418 Specifically, for classification problems, a positive SHAP value indicates that a given
419 input contributed to a positive classification and a negative value indicates the input
420 contributed to a low probability for a given classification.

421 422 **Data Records**

423
424 The LTS-US dataset⁵¹ is structured in a tabular format, where each row is a lake-year
425 combination. The main dataset is contained in “ensemble_predictions.csv” and is
426 structured in a way that provides both categorical LTS predictions as well as
427 probabilities for each LTS prediction. The probabilities reported in
428 “ensemble_predictions.csv” are averaged probabilities generated from each of the three
429 modeling methodologies. An additional tabular dataset (“individual_predictions.csv”)
430 contains probabilities generated for each of the three modeling methodologies and can
431 be merged with “ensemble_predictions.csv” by the “Hylak_id” and “year” columns.

432
433 We provide raw and average predicted LTS probabilities as well as variance among
434 models for a given LTS prediction to allow future users to filter predictions of a certain
435 threshold for their particular analysis. Although many thresholds may exist, reporting
436 probability thresholds used in subsequent analyses will help maintain reproducibility and
437 synthesis across studies. Below, we detail column names and metadata for each of the
438 core datasets contained within the LTS-US data product.

439
440 “ensemble_predictions.csv”

441
442 *Hylak_id*
443 HydroLAKES unique identifier of lake. Preserved from HydroLAKES input data to enable future
444 merging with HydroLAKES attributes.

445
446 *year*
447 Year, spans 1984 through 2020.

448

449 *categorical_ts*
450 Categorical predicted lake trophic state (i.e., oligo, eu/mixo, dys). Categorical prediction is
451 based on the highest probability among *mean_prob_dys*, *mean_prob_eumixo*, and
452 *mean_prob_oligo*.
453
454 *mean_prob_dys*
455 Probability that a lake-year combination is dystrophic. Probability is calculated by averaging
456 probabilities from all three modeling methods.
457
458 *mean_prob_eumixo*
459 Probability that a lake-year combination is eutrophic or mixotrophic. Probability is calculated by
460 averaging probabilities from all three modeling methods.
461
462 *mean_prob_oligo*
463 Probability that a lake-year combination is oligotrophic. Probability is calculated by averaging
464 probabilities from all three modeling methods.
465
466 *var_prob_dys*
467 Variance in probabilities among all three modeling methods that a given lake-year is dystrophic.
468
469 *var_prob_eumixo*
470 Variance in probabilities among all three modeling methods that a given lake-year is
471 eutrophic/mixotrophic.
472
473 *var_prob_oligo*
474 Variance in probabilities among all three modeling methods that a given lake-year is
475 oligotrophic.
476
477 *"individual_predictions.csv"*
478
479 *Hylak_id*
480 HydroLAKES unique identifier of lake. Preserved from HydroLAKES input data to enable future
481 merge with HydroLAKES attributes.
482
483 *year*
484 Year, spans 1984 through 2020.
485
486 *prob_dys_mlr*
487 Probability that a lake-year combination is dystrophic. Probability is calculated by multinomial,
488 multiple logistic regression.
489
490 *prob_eumixo_mlr*
491 Probability that a lake-year combination is eutrophic or mixotrophic. Probability is calculated by
492 multinomial, multiple logistic regression.
493
494 *prob_oligo_mlr*
495 Probability that a lake-year combination is oligotrophic. Probability is calculated by multinomial,
496 multiple logistic regression.
497
498 *prob_dys_mlp*

499 Probability that a lake-year combination is dystrophic. Probability is calculated by multilayer
500 perceptron.

501
502 *prob_eumixo_mlp*

503 Probability that a lake-year combination is eutrophic or mixotrophic. Probability is calculated by
504 multilayer perceptron.

505
506 *prob_oligo_mlp*

507 Probability that a lake-year combination is oligotrophic. Probability is calculated by multilayer
508 perceptron.

509
510 *prob_dys_xgb*

511 Probability that a lake-year combination is dystrophic. Probability is calculated by a gradient-
512 boosted regression.

513
514 *prob_eumixo_xgb*

515 Probability that a lake-year combination is eutrophic or mixotrophic. Probability is calculated by
516 a gradient-boosted regression.

517
518 *prob_oligo_xgb*

519 Probability that a lake-year combination is oligotrophic. Probability is calculated by a gradient-
520 boosted regression.

521
522 **Technical Validation**

523
524 *Model performance diagnostics*

525
526 To assess how each model correctly classified training data, we compared the model
527 accuracies, balanced accuracies, and AUC of ROC curves. Overall and balanced model
528 accuracies were similar, where all models had accuracies ranging from 72.4 to 72.9%
529 and balanced accuracies ranging from 69.9 to 71.5%. AUCs of ROCs were likewise
530 similar across all three model techniques, ranging from 0.88 to 0.90 (Figure S3). These
531 combined metrics suggest that all three modeling approaches performed similarly, when
532 assessing model performance with global metrics.

533
534 Although models performed similarly at high levels, they varied more in their robustness
535 to classify dystrophic lakes (Figure 3). Machine learning-based methods, such as
536 multilayer perceptron (60%) and gradient boosted regression (58%), had higher
537 balanced accuracies, whereas distribution-based methods, such as logistic regression
538 (55%), had lower balanced accuracies. These differences were largely driven by
539 deviations in true positive rates (47.5-50.6%), whereas true negative rates were higher
540 (91.8-92.7%). This difference in true negative and true positive rates is likely due to
541 spectral similarities between oligotrophic and dystrophic lakes, where both are
542 characterized by low primary production in comparison to eutrophic/mixotrophic lakes.
543 Although these differences only span 5%, they may be important, given that dystrophic
544 lakes tend to be uncommon relative to oligotrophic and eutrophic lakes²³. Such
545 differences imply variation in each model's robustness to predict rarer trophic states, but

546 our overall metrics of model performance highlight exceptional congruence across all
547 three modeling techniques.

548
549 *Spatial patterns in lake classification*

550
551 To evaluate spatio-temporal patterns in trophic state classification, we created spatial
552 confusion matrices, where predictions and reference sites were plotted across the entire
553 United States. We *a priori* hypothesized that when misclassifications result from lake-
554 specific deviations, misclassifications should be distributed throughout the United States
555 without any clear spatial patterns. In the event that spatial clustering of misclassified
556 lakes occurred, these patterns should be more pronounced where high densities of a
557 given lake trophic state are located. In cases when lake clustering appears in an
558 unexpected area, these patterns should be more attributed to place-based irregularities
559 in spectral data.

560
561 Confusion between oligotrophic and eutrophic/mixotrophic lakes were spatially
562 distributed throughout the entire continental United States, with no evidence of spatial
563 clustering (Figures S4-S6). In contrast, dystrophic misclassifications were broadly
564 isolated to the Upper Midwest and Upper Northeast regions. Consistent with our
565 hypotheses, these regions are associated with increased densities of dystrophic lakes,
566 suggesting that optical similarities between oligotrophic and dystrophic lakes in these
567 regions may lead to increased misclassification. Notably, dystrophic lakes tended to be
568 misclassified as oligotrophic, whereas oligotrophic lakes tended to not be misclassified
569 as dystrophic, meaning that our predictions should be conservative with assigning an
570 individual lake as dystrophic.

571
572 *Assessing patterns in lake classification*

573
574 Given that lake trophic state classifications may be a product of a lake's limnological,
575 morphological, and geographic properties, we performed a series of analyses of
576 variance (ANOVA) to test for significant differences (i.e., p-value < 0.05) in lake
577 classification accuracy. For each ANOVA, a lake property was the response variable,
578 and predictors were lake trophic state, model correctness (i.e., correct or incorrect
579 classification), and model type. All response variables were log-transformed to
580 approximate a normal distribution. Because each analysis had an unbalanced sample
581 size, we calculated Type II Sum-of-Squares⁵². Residuals for each model were assessed
582 for normality and homogeneity of variance.

583
584 The main goal of each ANOVA was to assess whether variation in a lake parameter
585 could be associated with variation in model methodologies, model correctness, or
586 trophic states themselves. Consequently, our ANOVAs do not include interaction terms,
587 as most interactions would not be helpful for understanding patterns in how our
588 classification models performed.

589
590 *NCP patterns in lake classification*

591

592 To assess how a lake's misclassification may be related to its position in the NCP, we
593 assessed where correctly and incorrectly classified lakes were located in the NCP.
594 Lakes that were incorrectly classified tended to be located near total phosphorus ($30 \pm$
595 $15 \mu\text{g/L}$) and color ($20 \pm 9 \text{ PCU}$) thresholds, with a large portion at the nexus of the total
596 phosphorus and color thresholds (Figure 4). Across all modeling techniques, correctly
597 classified lakes spanned a wider range across both axes, especially total phosphorus.
598 Median total phosphorus concentration for misclassified lakes was $24 \mu\text{g/L}$ (range: 1-
599 $4,772 \mu\text{g/L}$), whereas median total phosphorus concentration for correctly classified
600 lakes was $36 \mu\text{g/L}$ (range: 0.24- $4,144 \mu\text{g/L}$). Similarly, median PCU for correctly (14
601 PCU; range: 0-724 PCU) and incorrectly (16 PCU; range: 0-350 PCU) classified lakes
602 were along the edge of the color threshold of 20 PCU. When assessing total
603 phosphorus and color independently, ANOVA suggested that total phosphorus
604 concentrations were significantly different for correctly and incorrectly classified lakes,
605 whereas differences in color were not significantly different across correctly and
606 incorrectly classified lakes (Table 1; Figure 5).

607
608 Beyond total phosphorus and color patterns influencing lake classification, our analyses
609 of lakes that transitioned trophic states within a summer suggest that lakes along a NCP
610 boundary (i.e., near total phosphorus or color threshold) are more prone to
611 misclassification. Among lakes that transitioned within a summer, the most frequent
612 change in lake trophic state was among lakes switching from oligotrophic to eutrophic.
613 Considering that both total phosphorus concentrations as well as summertime lake
614 phenologies are associated with algal production that can optically obfuscate whether a
615 lake is oligotrophic or eutrophic, our results of NCP patterns are not surprising. Rather,
616 confusion along the total phosphorus axis of the NCP, an axis that corresponds with
617 autotrophic productivity, is concordant with the idea that a lake can experience
618 moments of eutrophy - e.g., a pulse of nutrients or algal growth - while otherwise being
619 oligotrophic for the majority of the summer. Therefore, classifications made for lakes at
620 the boundary of trophic states can be challenging, and our validation analyses describe
621 total phosphorus and color conditions where misclassifications may be more common.

622 623 *Morphological and locational patterns in lake classification*

624
625 At the spatial resolution of Landsat's sensors, there is a risk of "mixed pixels", where a
626 pixel includes water with fractions of adjacent bare land or vegetation. Given the
627 difference in optical contrast between water and other features, even minor differences
628 can lead to large errors in estimating surface reflectance. A major source of uncertainty
629 in lake optical water quality estimation is the separation of water and atmospheric
630 effects⁵³. The latter increases in severity near land and this adjacency effect can extend
631 several kilometers, depending on the state of the atmosphere.

632
633 Before assessing how edge and lakebed effects may influence model classifications, we
634 first ensured that spectral differences between each trophic state in our dataset were
635 greater than differences within a trophic state when accounting for lake area and depth.
636 To evaluate how edge and lakebed effects may be present within our training and test
637 data, we used lake area and average depth data from HydroLAKES³² as well as

638 maximum depth from the GloBathy dataset⁵⁴. While evaluating lake area, we noticed
639 that smaller lakes tended to have higher near-infrared relative reflectance values, and
640 relative near-infrared reflectance generally decreased with increasing lake area (Figures
641 S7-S8). Because LimnoSat-US aggregates reflectance data at the lake's Chebyshev
642 center, the point in the lake farthest away from shore, smaller lakes would likely have
643 Chebyshev centers that are closer to the shoreline. As terrestrial near-infrared
644 reflectances tend to be higher than aquatic near-infrared reflectances, smaller lakes
645 with Chebyshev centers closer to the shoreline may be associated with increased near-
646 infrared signatures. Similarly, relative blue reflectance increased with increasing lake
647 surface area, which would likewise be expected, as larger lakes likely have a
648 Chebyshev center that is farther from shore, and therefore, less influenced by shoreline
649 effects. With respect to lakebed effects, the shallowest lakes tended to have slightly
650 elevated relative green reflectance, which would be consistent with increased primary
651 production. Across all trophic states, lakes with average depths of 1-10 m were also
652 associated with increased relative near-infrared reflectance, suggesting that these lakes
653 may have the highest near-infrared reflectance due to reflectance signatures of lakebed
654 substrate or increased benthic algal production.

655 To evaluate how models might misclassify lakes in response to morphological and
656 geographic characteristics, we examined how lake depth, elevation, and surface area
657 may correspond to correct and incorrect classifications. Average and maximum lake
658 depth can be used to evaluate a lake's potential for lakebed effects, where reflectance
659 from benthic algae or sediment may confound signals for the actual surface of the lake.
660 Assessing classification differences across elevation ranges can be important for
661 understanding atmospheric effects on reflectance data, where higher elevations may
662 have fewer aerosols, and therefore contain fewer misclassifications. Lastly, examining
663 misclassifications across lake sizes can reveal potential for adjacency effects, where
664 surrounding geologies or vegetation may obscure surface reflectances observed over
665 the lake.

666
667 ANOVA results suggested that average depth, maximum depth, and elevation differed
668 significantly across correct and incorrect misclassifications (Table 2), although
669 differences based on average and maximum depth were more visually apparent than
670 those observed for elevation (Figure 6). In contrast, lake area did not differ significantly
671 across correct and incorrect classifications (Table 2).

672
673 Together, these analyses suggest that lakebed reflectance may lead to lake trophic
674 state misclassification, whereas edge effects are likely not consequential for inaccurate
675 lake trophic state classifications. In particular, shallower oligotrophic lakes (i.e., average
676 depth < 5 m and maximum depth < 15 m; Figure 6) and deeper eutrophic lakes (i.e.,
677 average depth > 5 m and maximum depth > 15 m; Figure 6) tended to be misclassified.
678 We speculate that these differences may stem from shallower, oligotrophic lakes having
679 pronounced benthic algal growth⁵⁵ that can produce a strong green signal. Conversely,
680 deeper eutrophic lakes may have less concentrated algal growth in the water column,
681 thereby creating a stronger blue reflectance relative to green reflectance and increasing
682 chances for misclassification (see *Optical patterns in lake classification*). Overall, these
683 results correspond with our NCP validation analyses, where total phosphorus

684 concentrations were associated with greater misclassifications of oligotrophic lakes as
685 eutrophic. Given the potential for lakes to be misclassified because of issues with
686 lakebed reflectance, considering whether depth could alter results and building
687 analytical workflows to assess sensitivity to interference from lakebed reflectance (see
688 *SHAP Analysis* for more detail) could improve model lake classifications.

689

690 *Optical patterns in lake classification*

691

692 To evaluate how models might misclassify lakes based on reflectance values, we
693 assessed how z-scored relative red, green, blue, and near-infrared reflectance values
694 differed between correctly and incorrectly predicted lake trophic state. Because we used
695 relative reflectances that are inherently interdependent, and thus violate ANOVA
696 assumptions, we elected to forgo significance tests for whether band ranges differed
697 across modeling methods.

698

699 For dystrophic lakes, incorrectly classified lakes, compared to correctly classified lakes,
700 tended to have lower z-scored near-infrared and blue band values as well as higher
701 green and red values (Figure 7). For eutrophic/mixotrophic lakes, misclassified lakes
702 tended to have lower values for red and green bands as well as higher values for blue
703 bands (Figure 7). For oligotrophic lakes, incorrectly classified lakes tended to have
704 higher red and lower blue band values (Figure 7).

705

706 These inconsistencies in LTS classification correspond with variation that can be
707 present in natural systems. Dystrophic lakes are generally characterized as having low
708 primary productivity and high dissolved organic matter, which should result in low green
709 band values as well as higher near-infrared values, yet misclassified dystrophic lakes
710 tended to have low near-infrared as well as high red and green bands. Eutrophic and
711 mixotrophic lakes are generally characterized as having high productivity, which should
712 result in high green values, yet misclassified eutrophic and mixotrophic lakes tended to
713 have low green and red as well as high blue bands. Oligotrophic lakes should be
714 characterized as having high blue bands, yet misclassified lakes tended to have low
715 blue and high red bands, which may be a product of bottom reflectance. Together,
716 these misclassifications likely represent lakes that are not characteristic of LTS
717 classifications. For example, a more productive oligotrophic lake could produce a
718 stronger red and green signature and, therefore, be classified as eutrophic. Likewise,
719 less productive eutrophic lakes may be optically more similar to oligotrophic lakes and,
720 therefore, be characterized by lower red and green bands.

721

722 *SHAP Analysis*

723

724 To evaluate the influence of remote sensing reflectance inputs on final predictions, we
725 assessed the distribution of SHAP values calculated for each predictor and for each
726 trophic state. In general, SHAP values can be useful for decoding how machine learning
727 and parametric methods may assign relative importance to a given predictor, thereby
728 increasing interpretability of a model. In an instance where models are classifying lakes
729 based on *a priori* hypothesized relationships, SHAP values across predictors should

730 correspond to the *a priori* hypothesized relationships. For example, oligotrophic lakes
731 are generally characterized as having high blue reflectance relative to red and green,
732 and in a case where models reflect this understanding, SHAP values should attribute an
733 oligotrophic classification to high values in the relative blue reflectance. Consistently
734 high attributions for blue reflectances should subsequently result in high overall feature
735 importance when discriminating oligotrophic lakes.

736
737 When evaluating feature importance across trophic states, measured as the mean
738 absolute SHAP value of a given feature, all models agreed on the most influential
739 features for classification (Figure S9). Furthermore, the distribution of SHAP values
740 reflected limnological understanding of each trophic state's inherent properties. For
741 dystrophic lakes, SHAP values indicate that models relied on low green and high near-
742 infrared and red band values, corroborating the idea that dystrophic lakes should have
743 lower primary production and increased CDOM^{21,56} (Figure S9). Predictions for
744 eutrophic and mixotrophic lakes were attributed to high red and low blue band values,
745 corresponding with the idea that eutrophic and mixotrophic lakes should have higher
746 algal production²³ (Figure S9). Conversely, SHAP values for oligotrophic lakes attributed
747 predictions to low red and high blue band values, agreeing with the idea that
748 oligotrophic lakes should have lower algal production²³ (Figure S9). Beyond each
749 individual trophic state's most important predictors, our SHAP analysis mirrored the
750 logic of NCP analyses, where lakes with lower true color values (i.e., oligotrophic and
751 eutrophic) were discriminated more effectively by bands associated with autotrophic
752 capacity, whereas lakes with higher true color values (i.e., dystrophic) were
753 discriminated more effectively by bands suggesting decreased autotrophic production
754 and increased colored dissolved organic carbon.

755
756 SHAP values can also provide insight on what drives models to misclassify certain
757 lakes. Specifically, when examining smaller, shallower oligotrophic lakes that could
758 potentially be influenced by bottom reflectance or adjacency effects, we observed that
759 some misclassifications were attributable to models relying on low relative blue
760 reflectance and high relative near-infrared reflectance (Figures S10-S15). These
761 patterns indicate that in certain lakes, the models were unable to distinguish the spectral
762 signatures that are potentially attributable to sediment or benthic algae as well as
763 shoreline vegetation and soil. The spectral similarity between shallow oligotrophic and
764 deep eutrophic lakes is relevant to active research trajectories in limnology, particularly
765 those examining the relatively high contributions of benthic algal communities to whole
766 lake productivity in oligotrophic lakes^{55,57-60}. Given the potential for lakebed effects to
767 alter classifications, research questions could consider the influence of depth-related
768 misclassifications.

769 *Comparing predicted and NLA spatial patterns*

770
771 To independently validate the LTS-US dataset's robustness in capturing macroscale
772 and multi-year changes in lake trophic state, we replicated analyses similar to Leech et
773 al.²³ and compared statistics from the NLA with those from the LTS-US dataset. We first
774 merged the lake trophic state classifications from the 2007, 2012, and 2017 NLA
775

776 campaigns as well as the LTS-US dataset with the U.S. EPA Level I Ecoregions²⁹. We
777 then calculated the proportion of each trophic state occurring within each ecoregion in a
778 given year. To compare the NLA and the LTS-US dataset, we calculated the absolute
779 difference between predicted and estimated proportions for each trophic state within
780 each year and ecoregion.

781
782 Predicted and measured proportions were broadly consistent across all three years.
783 Visually, all three years and trophic states followed consistent trends across all
784 ecoregions (Figure 8). For example, our models generally captured increasing
785 dystrophic and decreasing oligotrophic lakes in northern forested regions, a pattern
786 consistent with Leech et al.²³. Absolute differences between estimated and predicted
787 proportions across ecoregions were likewise congruent across all three years.
788 Eutrophic/mixotrophic lakes tended to have the smallest differences (mean = -5.3%, sd
789 = 19%), indicating that our models may overestimate relative abundance of eutrophic
790 and mixotrophic lakes (Figure S16). In contrast, dystrophic (mean = 7.0%, sd = 6.7%)
791 and oligotrophic (mean = 7.6%, sd = 22.4%) relative abundance tended to be
792 underestimated (Figure S16). Larger standard deviation values were caused by some
793 ecoregions having few lakes overall, thereby increasing proportions of a given trophic
794 state within an ecoregion. When filtering for ecoregions that contained at least 10 lakes,
795 we noticed similar patterns of eutrophic and mixotrophic lakes being slightly
796 overestimated (mean = -7.9%, sd = 11.3%), as well as dystrophic (mean = 9.1%, sd =
797 6.7%) and oligotrophic (mean = 4.6%, sd = 13.8%) lakes being underestimated; yet the
798 standard deviation in absolute differences decreased.

799
800 Together, these analyses demonstrate that though the LTS-US dataset does contain
801 biases towards eutrophic/mixotrophic classification, its overall congruence with the NLA
802 highlights its robustness. These biases may stem from our models attempting to classify
803 lake ecosystem properties based on optically visible (i.e., color) and optically invisible
804 (i.e., phosphorus) properties, where the exceptionally oligotrophic, dystrophic, and
805 eutrophic/mixotrophic lakes are more consistently discriminated. In contrast, the NLA
806 may likewise contain biases due to site selection, whereas our methods select for all
807 lakes of at least 10 ha in area. Regardless of the biases in the LTS-US and NLA
808 datasets, the congruence between the two is even more notable considering that our
809 modeling approaches and the NLA use independent methods for classifying lake trophic
810 state. The NLA uses *in situ* total phosphorus and true color measurements, whereas our
811 methods use lake red, green, blue, and near-infrared reflectance. Furthermore, despite
812 not including temporal or spatial predictors, our models reproduce NLA spatial and
813 temporal trends in lake trophic state at the spatial and temporal scales.

814
815 Given both the potential biases and robustness of the LTS-US data product, cross-
816 referencing the LTS-US dataset with known trends in an area of interest, especially in
817 areas where lakes may be less abundant could enhance regional and local analyses. In
818 instances where the LTS-US dataset may be more biased, reproducing the LTS-US
819 dataset using both our existing code and particular predictors of interest for a region,
820 such as average depth, lake area, or watershed area could offer particular insights into
821 why a given region may be more prone to misclassification. Creating tailored versions

822 of the core LTS-US dataset can promote further understanding of multi-scale features
823 that may be important for assessing lake trophic state with remotely sensed surface
824 reflectance data.

825 826 *Manual Quality Control*

827
828 To ensure integrity of lake classifications across all steps of our pipeline, we
829 subsampled 250 lakes from the final dataset and manually cross-referenced their
830 predicted trophic state with independent sources. The random subsample only included
831 lakes that had associated names in the HydroLAKES dataset and was stratified by lake
832 surface area, where surface areas were binned by orders of magnitude (i.e., $< 1 \text{ km}^2$,
833 $(1, 10] \text{ km}^2$, $(10, 100] \text{ km}^2$, $(100, 1,000] \text{ km}^2$, $(1,000, 10,000] \text{ km}^2$, $> 10,000 \text{ km}^2$). We
834 filtered specifically for lakes with names because we assumed that named lakes within
835 the HydroLAKES database would likely have more publicly available information about
836 their water quality and would likely be easier to find within managerial reports and
837 scientific publications.

838
839 To minimize bias, persons engaged in manual checking only received lake latitude and
840 longitude, name, and the U.S. state where the lake was located. All persons engaged in
841 manual checking were not involved in model and prediction development and were,
842 therefore, blind to individual lake predictions. When possible, persons identified trophic
843 states for multiple years, although many sources only referenced a lake's trophic state
844 in an individual year or broadly across multiple years. In either case, LTS was reported
845 for the lake and years that independent sources reported.

846
847 Of the 250 target lakes, we were able to find verified trophic state data on 93 lakes
848 (38%). For the 93 lakes that had independent lake trophic state data, our models
849 corroborated independent, *in situ* observations 74% of the time, which is consistent with
850 our models' overall accuracy against testing data from the U.S. EPA NLA. We did not
851 observe any apparent spatial patterns with model misclassification, which complements
852 our spatial confusion validation (Figure S17). Together, these results demonstrate that
853 our manual checking procedure returned similar results as our evaluation procedures
854 against our testing data, giving confidence that our modeling pipeline and evaluation
855 procedures are both robust and able to capture natural processes occurring in lakes.

856 857 *Effects of processor heterogeneity*

858
859 When recreating lake trophic state predictions *de novo*, care should be taken to ensure
860 that effects from heterogeneous processors are minimized. When creating the LTS-US
861 dataset from the original LimnoSat-US dataset³⁴, we specified seeds for each modeling
862 framework, which enabled us to reproduce results between model runs. Final dataset
863 production occurred on one machine using an Intel(R) Xeon(R) W-10885M processor
864 with eight cores, however, slight differences may arise due to differences in a user's
865 hardware float precision.

866

867 If users recreate or update LimnoSat-US prior to recreation of the LTS-US predictions,
868 care should be taken as Google Earth Engine⁶¹ uses a heterogeneous processor
869 framework, where individual processors cannot currently be specified. Meyer et al.⁹
870 quantified the effect of Google Earth Engine's processor heterogeneity on various lake
871 surface area and basin-level climatological estimations, and effects of processor
872 heterogeneity were likely inconsequential (e.g., differences of 10⁻¹²), although these
873 differences may result in slightly different trophic state predictions. The extent to which
874 these values would influence results or conclusions of other studies will depend on the
875 level of precision required and scope of research question.

876 877 **Usage Notes**

878
879 The LTS-US dataset was constructed to be an accessible and interoperable product for
880 a range of basic and applied research questions related to water quality and ecological
881 integrity at national scales. Here, we detail several options for application of the LTS-US
882 dataset and associated pipeline.

883
884 First, the LTS-US dataset can be joined with water quantity and quality datasets to
885 assess how changes in LTS, and therefore ecosystem integrity, may be influenced by
886 watershed processes, climate, and human population. At the local scale, the LTS-US
887 dataset can be merged with *in situ* sampling data or modeled data from individual lakes
888 to assess how hydrodynamic, climatic, physicochemical, and biological processes may
889 be associated with interannual variation in LTS. As demonstrated here, local *in situ*
890 observations are important for providing validation of the LTS data, and potentially,
891 refinement of methods for deriving LTS predictions. Similarly, the LTS-US dataset can
892 be merged with data from research coordination networks, such as the National
893 Ecological Observatory Network (www.neonscience.org) or the Global Lake Ecological
894 Observatory Network⁶², to enable upscaling highly localized processes to regional and
895 national scales. Beyond watershed-specific processes, the LTS-US dataset can likewise
896 be useful for synthetic questions focused on macroscale water quality trends. For
897 example, in cases where users may wish to synthesize changes in lake ecosystem
898 metabolism with trends in lake water quantity, climate, and human population, the LTS-
899 US dataset can be merged with the GLCP (Global Lake area, Climate, and Population)⁹
900 or LakeATLAS⁶³, thereby enabling users to assess how changes in seasonal and
901 permanent lake surface area may correlate with changes in lake trophic state. The LTS-
902 US dataset offers a valuable resource for addressing a broad spectrum of basic and
903 applied research questions from local and regional to continental scales.

904
905 Second, the LTS-US dataset provides a tool for using remote sensing products with the
906 NCP, a framework increasingly used by limnologists, to understand lake water quality at
907 macroscales. Although previous studies have remotely sensed lake trophic state
908 index⁶⁴, our data product is the first to incorporate NCP with remote sensing reflectance
909 data. Where TSI focuses exclusively on eutrophication patterns (also known as
910 greening) associated with nutrient-driven primary production, the LTS-US dataset
911 enables investigations of the spatial extent and temporal trends of lake dystrophication
912 (also known as lake browning). This difference between TSI and NCP is important for

913 assessing long term and spatially extensive changes in lake browning, as well as
914 “murkification” (i.e. simultaneous browning and greening), which has been associated
915 with complex, often non-linear changes in temperature, pH, dissolved oxygen, and food
916 web structure^{23,56}. Further, national-scale sampling campaigns, such as the U.S. EPA
917 NLA, have helped reveal that the proportion of dystrophic lakes has been increasing
918 nationally since 2007²³. The U.S. EPA NLA is one of the most extensive, structured, and
919 coordinated lake sampling efforts at the national scale, and the LTS-US dataset can
920 complement these *in situ* data by providing finer temporal information at comparable
921 spatial scales. When data from successive NLA sampling campaigns become available,
922 the LTS-US dataset can be updated and further benefit from additional training data.
923 Together, the use of remote sensing imagery with extensive sampling campaigns, like
924 the NLA, can be useful for identifying broadscale changes in water quality.

925
926 Third, although our reflectance data are spatially aggregated to represent each lake’s
927 characteristic summertime reflectances, our data pipeline and modeling frameworks are
928 amenable to numerous data aggregations, thereby enabling investigation of lakes’ intra-
929 and inter-annual phenologies. For example, many oligotrophic lakes experience
930 summertime greening, due to increased algal growth throughout the summer. Although
931 algal succession tends to follow similar temporal and community compositional
932 patterns^{65,66}, users may be interested in understanding how greening events may shift
933 temporally in response to climatic and anthropogenic disturbances. Similarly, end users
934 may be interested in understanding intra-lake heterogeneities, where embayments or
935 nearshore areas may differ in trophic state from the offshore. In both cases, users could
936 adapt our data, modeling, and validation pipeline, where temporal and spatial resolution
937 are more finely resolved. Operationally, end users could modify the aggregation scripts
938 (“1_aggregate.R” and “aggregate_utils.R”)⁵¹ and LimnoSat codes³⁴ to accommodate
939 input data that aggregate at monthly or fortnightly timesteps as well as on a per-pixel
940 basis. Because our data pipeline allows for automated re-running of all harmonization,
941 modeling, and quality control routines, users are able to build off of the existing
942 infrastructure to tailor the LTS-US dataset to their particular research questions without
943 high computational overhead or the need to build new workflows *de novo*.

944
945 Beyond any specific research question, the LTS-US dataset is a streamlined resource
946 for many end users looking to incorporate remote sensing and its derived products into
947 their analyses. Because of the dataset’s interoperability and flexible structure, the LTS-
948 US dataset serves as a powerful resource for evaluating and contextualizing aquatic
949 ecosystem change at local-to-national spatial as well as annual-to-decadal temporal
950 scales.

951 **Code Availability**

952
953
954 All data harmonization, modeling, and validation procedures for the LTS-US dataset
955 were scripted in the R Statistical Environment⁶⁷, using the tidyverse⁶⁸, lubridate⁶⁹,
956 data.table⁷⁰, sf⁷¹, keras⁷², tensorflow⁷³, caret⁷⁴, CAST⁷⁵, yaml⁷⁶, reticulate⁷⁷, xgboost⁷⁸,
957 nnet⁴⁴, viridis⁷⁹, trend⁸⁰, multiROC⁸¹, ggpubr⁸², fastshap⁸³, maps⁸⁴, ggtext⁸⁵, and
958 ggforce⁸⁶ packages.

959
960 To enhance reproducibility, all scripts are designed to work within a single pipeline that
961 uses the targets package⁸⁷. The targets pipeline is divided into four main components:
962 “1_aggregate”, “2_train”, “3_predict”, and “4_qc”. Each component corresponds to one
963 of the steps presented above and can be customized by users to fit their specific needs.
964 The associated pipeline setup and user guide can be found on the Environmental Data
965 Initiative⁵¹, where the “README_targets.pdf” file details directory architecture and how
966 to execute the pipeline.

967
968 To ensure reproducibility across operating platforms, all scripts for the pipeline can be
969 executed within a container. Running the pipeline within the container allows users to
970 execute the entire pipeline without the need to make small, yet important, edits to the
971 code, or to configure their own operating environment to conform to the pipeline’s
972 requirements. For example, recent versions of the sf package default to using the s2
973 spherical geometry engine instead of the Graphic Environment Operating System
974 (GEOS), which assumes planar coordinates. End users on a system with one version of
975 the sf library might need to adjust the code to use the correct geometry engine, whereas
976 users with another version might be able to run the pipeline without any adjustments.
977 The container crystallizes a known-working set of libraries, both at the system level (e.g.
978 GEOS, GDAL, PROJ) and at the R level (e.g. sf), so that anybody can run the code
979 without reconfiguring their own environment. This also provides future proofing by
980 ensuring that the inevitable changes to other libraries over time do not lead to errors. To
981 help end users, who are less familiar with running containerized code, a tutorial for
982 installing and executing the pipeline within the container is located in the Environmental
983 Data Initiative repository as a compressed entity (see “README_container.pdf”)⁵¹.

984 985 **Acknowledgements**

986
987 We would like to thank Jennifer C. Adam, Julian J. Reyes, Paul C. Hanson, Austin P.
988 Delany, and Cee Nell for diverse technical and creative support during the production of
989 the LTS-US dataset. We would like to thank Joshua Culpepper and Lauren Koenig for
990 reviewing the LTS-US data product’s data, code, and metadata. Additionally, we would
991 like to thank John R. Gardner and Jida Wang for providing insightful comments and
992 feedback on a previous version of this manuscript. MFM, SNT, and KCF were
993 supported by Mendenhall Fellowships from the U.S. Geological Survey. RMP was
994 supported by the U.S. Department of Energy (DOE), Office of Energy Efficiency and
995 Renewable Energy, Water Power Technologies Office, and Environmental Sciences
996 Division at Oak Ridge National Laboratory (ORNL). ORNL is managed by UT-Battelle,
997 LLC, for the U.S. DOE under contract DE-AC05-00OR22725. IAO was supported by
998 NSF award #EPS-2019528. RIW was supported by a UKRI Natural Environment
999 Research Council (NERC) Independent Research Fellowship [grant number
1000 NE/T011246/1]. The National Lakes Assessment 2007, 2012, and 2017 data were a
1001 result of the collective efforts of dedicated field crews, laboratory staff, data
1002 management and quality control staff, analysts and many others from the U.S. EPA,
1003 states, tribes, federal agencies, universities, and other organizations. Any use of trade,

1004 firm, or product names is for descriptive purposes only and does not imply endorsement
1005 by the U.S. Government.

1006

1007 **Author Contributions**

1008

1009 MFM, SNT, TVK, JRE, and MRVR conceived the idea of the manuscript. MFM, TVK,
1010 SEH, and DML designed the manuscript. MFM provided leadership for the project and
1011 also performed all data harmonization. MFM, SNT, RL, JCR, and XY contributed to
1012 model development. MFM and SNT performed high-level validation checks for the data
1013 and models. TVK, RL, RMP, JRE, and JR conducted manual quality control. IAO, JCR,
1014 MRVR, RIW, and MRB reproduced coding routines. MFM, SNT, RMP, HAD, IAO, and
1015 RIW drafted figures and/or tables. MFM, SNT, RL, RMP, HAD, SEH, DML, IAO, JCR,
1016 RIW, XY, KCF, JCP, and AIP wrote original parts of the manuscript. All authors
1017 performed critical review and editing of the manuscript. All authors read and approved
1018 the final manuscript.

1019

1020 **Competing Interests**

1021

1022 The authors declare no competing interests.

1023 **References**

- 1024
- 1025 1. Mekonnen, M. M. & Hoekstra, A. Y. Four billion people facing severe water scarcity.
- 1026 *Science Advances* **2**, e1500323 (2016).
- 1027 2. Topp, S. N. *et al.* Shifting Patterns of Summer Lake Color Phenology in Over 26,000 US
- 1028 Lakes. *Water Resources Research* **57**, e2020WR029123 (2021).
- 1029 3. Topp, S. N. *et al.* Multi-decadal improvement in US Lake water clarity. *Environ. Res. Lett.*
- 1030 **16**, 055025 (2021).
- 1031 4. Kuhn, C. & Butman, D. Declining greenness in Arctic-boreal lakes. *Proceedings of the*
- 1032 *National Academy of Sciences* **118**, e2021219118 (2021).
- 1033 5. Paltsev, A. & Creed, I. F. Are Northern Lakes in Relatively Intact Temperate Forests
- 1034 Showing Signs of Increasing Phytoplankton Biomass? *Ecosystems* **25**, 727–755 (2022).
- 1035 6. Zhao, G., Li, Y., Zhou, L. & Gao, H. Evaporative water loss of 1.42 million global lakes. *Nat*
- 1036 *Commun* **13**, 3686 (2022).
- 1037 7. Oleksy, I. A. *et al.* Heterogenous controls on lake color and trends across the high-elevation
- 1038 U.S. Rocky Mountain region. *Environ. Res. Lett.* **17**, 104041 (2022).
- 1039 8. Pekel, J.-F., Cottam, A., Gorelick, N. & Belward, A. S. High-resolution mapping of global
- 1040 surface water and its long-term changes. *Nature* **540**, 418–422 (2016).
- 1041 9. Meyer, M. F., Labou, S. G., Cramer, A. N., Brousil, M. R. & Luff, B. T. The global lake area,
- 1042 climate, and population dataset. *Sci Data* **7**, 174 (2020).
- 1043 10. Khandelwal, A. *et al.* ReaLSAT, a global dataset of reservoir and lake surface area
- 1044 variations. *Sci Data* **9**, 356 (2022).
- 1045 11. Carrea, L. *et al.* Satellite-derived multivariate world-wide lake physical variable timeseries
- 1046 for climate studies. *Sci Data* **10**, 30 (2023).
- 1047 12. Gardner, J. R. *et al.* The Color of Rivers. *Geophysical Research Letters* **48**,
- 1048 e2020GL088946 (2021).

- 1049 13. Yang, X. *et al.* The Color of Earth's Lakes. *Geophysical Research Letters* **49**,
1050 e2022GL098925 (2022).
- 1051 14. Kraemer, B. M., Kakouei, K., Munteanu, C., Thayne, M. W. & Adrian, R. Worldwide
1052 moderate-resolution mapping of lake surface chl-a reveals variable responses to global
1053 change (1997–2020). *PLOS Water* **1**, e0000051 (2022).
- 1054 15. Hou, X. *et al.* Global mapping reveals increase in lacustrine algal blooms over the past
1055 decade. *Nat. Geosci.* **15**, 130–134 (2022).
- 1056 16. Read, E. K. *et al.* Water quality data for national-scale aquatic research: The Water Quality
1057 Portal. *Water Resources Research* **53**, 1735–1745 (2017).
- 1058 17. Ross, M. R. V. *et al.* AquaSat: A Data Set to Enable Remote Sensing of Water Quality for
1059 Inland Waters. *Water Resources Research* **55**, 10012–10025 (2019).
- 1060 18. USEPA. *The National Eutrophication Survey*. (1972).
- 1061 19. Ledesma, J. L. J., Köhler, S. J. & Futter, M. N. Long-term dynamics of dissolved organic
1062 carbon: Implications for drinking water supply. *Science of The Total Environment* **432**, 1–11
1063 (2012).
- 1064 20. Carlson, R. E. A trophic state index for lakes. *Limnology and Oceanography* **22**, 361–369
1065 (1977).
- 1066 21. Williamson, C. E., Morris, D. P., Pace, M. L. & Olson, O. G. Dissolved organic carbon and
1067 nutrients as regulators of lake ecosystems: Resurrection of a more integrated paradigm.
1068 *Limnology and Oceanography* **44**, 795–803 (1999).
- 1069 22. Webster, K. E. *et al.* An empirical evaluation of the nutrient-color paradigm for lakes.
1070 *Limnology and Oceanography* **53**, 1137–1148 (2008).
- 1071 23. Leech, D. M., Pollard, A. I., Labou, S. G. & Hampton, S. E. Fewer blue lakes and more
1072 murky lakes across the continental U.S.: Implications for planktonic food webs. *Limnology
1073 and Oceanography* **63**, 2661–2680 (2018).
- 1074 24. USEPA. *Survey of the Nation's Lakes. Field Operations Manual*. (2007).

- 1075 25. USEPA. *2012 National Lakes Assessment. Field Operations Manual*. (2011).
- 1076 26. USEPA. *National Lakes Assessment 2017. Field Operations Manual*. (2017).
- 1077 27. USEPA. *National Lakes Assessment. Laboratory Operations Manual*. (2012).
- 1078 28. USEPA. *National Lakes Assessment 2017. Laboratory Operations Manual. V.1.1.1*. (2017).
- 1079 29. Omernik, J. M. Ecoregions of the Conterminous United States. *Annals of the Association of*
1080 *American Geographers* **77**, 118–125 (1987).
- 1081 30. USEPA. *Handbook of Methods for Acid Deposition Studies: Laboratory Analyses for*
1082 *Surface Water Chemistry*. (U.S. Environmental Protection Agency, Office of Research and
1083 Development, 1987).
- 1084 31. APHA. *Standard Methods for the Examination of Water and Wastewater. American Public*
1085 *Health Association, Washington DC*. (American Public Health Association, 1999).
- 1086 32. Messenger, M. L., Lehner, B., Grill, G., Nedeva, I. & Schmitt, O. Estimating the volume and
1087 age of water stored in global lakes using a geo-statistical approach. *Nat Commun* **7**, 13603
1088 (2016).
- 1089 33. Robinson, N., Regetz, J. & Guralnick, R. P. EarthEnv-DEM90: A nearly-global, void-free,
1090 multi-scale smoothed, 90m digital elevation model from fused ASTER and SRTM data.
1091 *ISPRS Journal of Photogrammetry and Remote Sensing* **87**, 57–67 (2014).
- 1092 34. Topp, S., Pavelsky, T., Yang, X., Gardner, J. & Ross, M. R. V. LimnoSat-US: A Remote
1093 Sensing Dataset for U.S. Lakes from 1984-2020. (2020) doi:10.5281/zenodo.4139695.
- 1094 35. Shen, Z., Yu, X., Sheng, Y., Li, J. & Luo, J. A Fast Algorithm to Estimate the Deepest Points
1095 of Lakes for Regional Lake Registration. *PLOS ONE* **10**, e0144700 (2015).
- 1096 36. Jones, J. W. Improved Automated Detection of Subpixel-Scale Inundation—Revised
1097 Dynamic Surface Water Extent (DSWE) Partial Surface Water Tests. *Remote Sensing* **11**,
1098 374 (2019).
- 1099 37. Foga, S. *et al.* Cloud detection algorithm comparison and validation for operational Landsat
1100 data products. *Remote Sensing of Environment* **194**, 379–390 (2017).

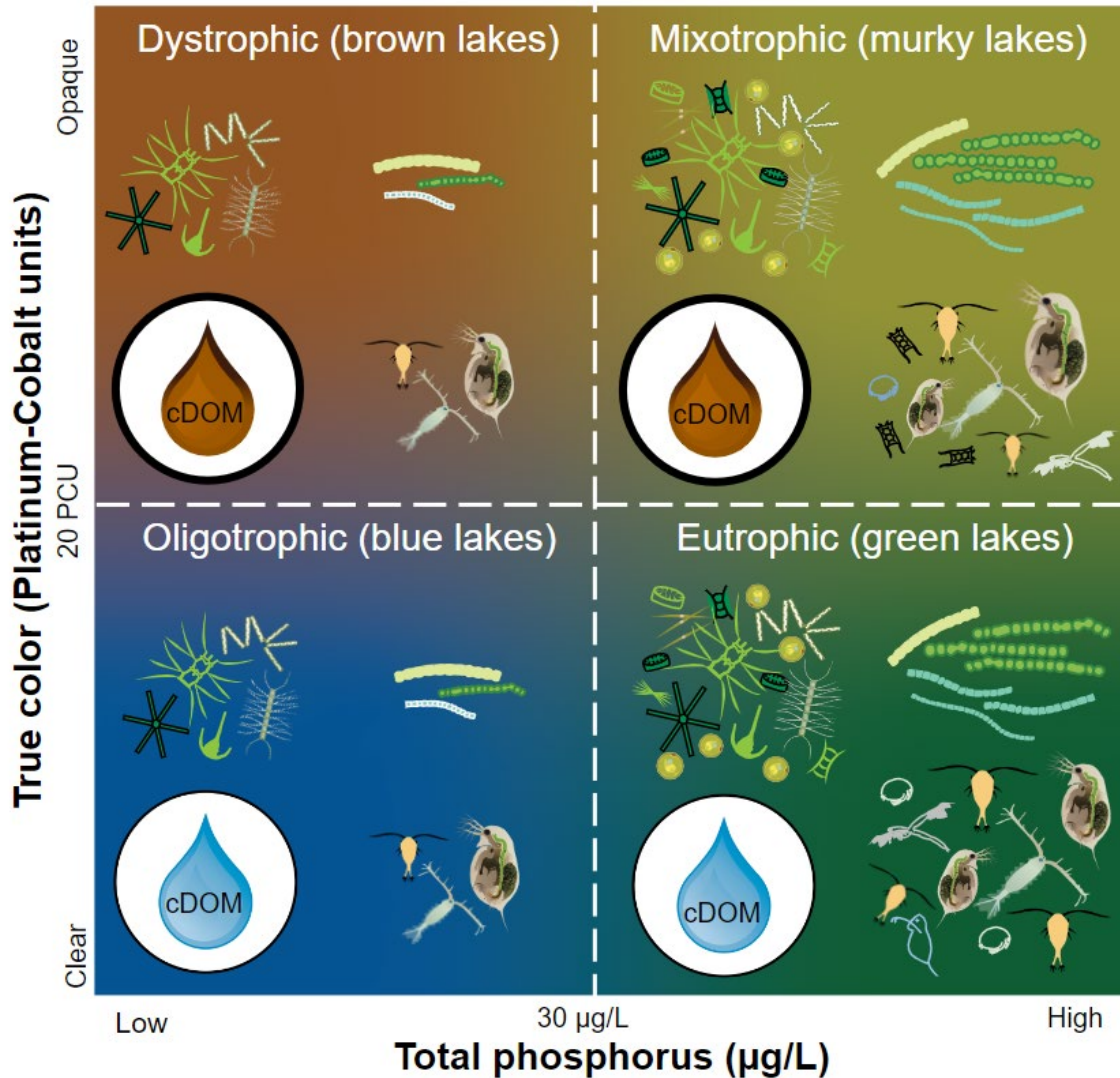
- 1101 38. Naumann, E. Undersökningar över fytoplankton och under den pelagiska regionen
1102 fösiggående gyttje-och dybildningar inom vissa syd- och mellansvenska urbergsvatten. *K.*
1103 *Sv. Vetensk. Akad. Handl.* **56**, 1–165 (1917).
- 1104 39. Thienemann, A. Seetyper. *Naturwissenschaften* **9**, (1921).
- 1105 40. Järnefelt, H. Zur Limnologie einiger Gewässer Finnlands. *Soc. Zool. Bot. Fennicae Vanamo*
1106 **2**, 185–352 (1925).
- 1107 41. Rohde, W. Crystallization of Eutrophication Concepts in Northern Europe. in *Eutrophication:*
1108 *Causes, Consequences, Correctives* 20256 (National Academies Press, 1969).
1109 doi:10.17226/20256.
- 1110 42. Nürnberg, G. K. & Shaw, M. Productivity of clear and humic lakes: nutrients, phytoplankton,
1111 bacteria. *Hydrobiologia* **382**, 97–112 (1998).
- 1112 43. Wetzel, R. G. *Limnology: Lake and River Ecosystems*. (Academic Press, 2001).
- 1113 44. Venables, W. N. & Ripley, B. D. *Modern Applied Statistics with S*. (Springer, 2002).
- 1114 45. Friedman, J. H. Greedy function approximation: A gradient boosting machine. *The Annals of*
1115 *Statistics* **29**, 1189–1232 (2001).
- 1116 46. Rosenblatt, F. The perceptron: A probabilistic model for information storage and
1117 organization in the brain. *Psychological Review* **65**, 386–408 (1958).
- 1118 47. Willard, J. D. *et al.* Predicting Water Temperature Dynamics of Unmonitored Lakes With
1119 Meta-Transfer Learning. *Water Resources Research* **57**, e2021WR029579 (2021).
- 1120 48. Shapley, L. S. 17. A Value for n-Person Games. in *Contributions to the Theory of Games*
1121 *(AM-28), Volume II* (eds. Kuhn, H. W. & Tucker, A. W.) 307–318 (Princeton University
1122 Press, 1953). doi:doi:10.1515/9781400881970-018.
- 1123 49. Štrumbelj, E. & Kononenko, I. Explaining prediction models and individual predictions with
1124 feature contributions. *Knowl Inf Syst* **41**, 647–665 (2014).

- 1125 50. Lundberg, S. M. & Lee, S.-I. A Unified Approach to Interpreting Model Predictions. in
1126 *Advances in Neural Information Processing Systems* (eds. Guyon, I. et al.) vol. 30 (Curran
1127 Associates, Inc., 2017).
- 1128 51. Meyer, M. F. *et al.* National-scale, remotely sensed lake trophic state (LTS-US) 1984-2020.
1129 *Environmental Data Initiative* (2023)
1130 doi:<https://doi.org/10.6073/pasta/212a3172ac36e8dc6e1862f9c2522fa4>.
- 1131 52. Langsrud, Ø. ANOVA for unbalanced data: Use Type II instead of Type III sums of squares.
1132 *Statistics and Computing* **13**, 163–167 (2003).
- 1133 53. Pahlevan, N. *et al.* ACIX-Aqua: A global assessment of atmospheric correction methods for
1134 Landsat-8 and Sentinel-2 over lakes, rivers, and coastal waters. *Remote Sensing of*
1135 *Environment* **258**, 112366 (2021).
- 1136 54. Khazaei, B., Read, L. K., Casali, M., Sampson, K. M. & Yates, D. N. GLOBathy, the global
1137 lakes bathymetry dataset. *Sci Data* **9**, 36 (2022).
- 1138 55. Vadeboncoeur, Y., Peterson, G., Zanden, M. J. V. & Kalff, J. Benthic Algal Production
1139 across Lake Size Gradients: Interactions among Morphometry, Nutrients, and Light. *Ecology*
1140 **89**, 2542–2552 (2008).
- 1141 56. Williamson, C. E. *et al.* Ecological consequences of long-term browning in lakes. *Scientific*
1142 *Reports* **5**, 1–10 (2015).
- 1143 57. Rosenberger, E. E., Hampton, S. E., Fradkin, S. C. & Kennedy, B. P. Effects of shoreline
1144 development on the nearshore environment in large deep oligotrophic lakes. *Freshwater*
1145 *Biology* **53**, 1673–1691 (2008).
- 1146 58. Hampton, S. E. *et al.* Disproportionate importance of nearshore habitat for the food web of a
1147 deep oligotrophic lake. *Mar. Freshwater Res.* **62**, 350–358 (2011).
- 1148 59. Atkins, K. S. *et al.* Integrating periphyton and surface water–groundwater methods to
1149 understand lake ecosystem processes. *Limnology and Oceanography: Methods* **20**, 61–88
1150 (2022).

- 1151 60. Meyer, M. F. *et al.* Effects of spatially heterogeneous lakeside development on nearshore
1152 biotic communities in a large, deep, oligotrophic lake. *Limnology and Oceanography* **67**,
1153 2649–2664 (2022).
- 1154 61. Gorelick, N. *et al.* Google Earth Engine: Planetary-scale geospatial analysis for everyone.
1155 *Remote Sensing of Environment* **202**, 18–27 (2017).
- 1156 62. Weathers, K. C. *et al.* The Global Lake Ecological Observatory Network (gleon): The
1157 Evolution of Grassroots Network Science. *Limnology and Oceanography Bulletin* **22**, 71–73
1158 (2013).
- 1159 63. Lehner, B., Messenger, M. L., Korver, M. C. & Linke, S. Global hydro-environmental lake
1160 characteristics at high spatial resolution. *Sci Data* **9**, 351 (2022).
- 1161 64. Gilarranz, L. J., Narwani, A., Odermatt, D., Siber, R. & Dakos, V. Regime shifts, trends, and
1162 variability of lake productivity at a global scale. *Proceedings of the National Academy of*
1163 *Sciences* **119**, e2116413119 (2022).
- 1164 65. Sommer, U., Gliwicz, Z. M., Lampert, W. & Duncan, A. The PEG-model of seasonal
1165 succession of planktonic events in fresh waters. *Archiv für Hydrobiologie* **106**, 433–471
1166 (1986).
- 1167 66. Sommer, U. *et al.* Beyond the Plankton Ecology Group (PEG) Model: Mechanisms Driving
1168 Plankton Succession. *Annual Review of Ecology, Evolution, and Systematics* **43**, 429–448
1169 (2012).
- 1170 67. R Core Team. *R: A Language and Environment for Statistical Computing*. (R Foundation for
1171 Statistical Computing, 2022).
- 1172 68. Wickham, H. *et al.* Welcome to the tidyverse. *Journal of Open Source Software* **4**, 1686
1173 (2019).
- 1174 69. Grolemund, G. & Wickham, H. Dates and Times Made Easy with lubridate. *Journal of*
1175 *Statistical Software* **40**, 1–25 (2011).
- 1176 70. Dowle, M. & Srinivasan, A. *data.table: Extension of `data.frame`*. (2021).

- 1177 71. Pebesma, E. Simple Features for R: Standardized Support for Spatial Vector Data. *The R*
1178 *Journal* **10**, 439–446 (2018).
- 1179 72. Allaire, J. J. & Chollet, F. *keras: R Interface to 'Keras'*. (2022).
- 1180 73. Allaire, J. J. & Tang, Y. *tensorflow: R Interface to 'TensorFlow'*. (2022).
- 1181 74. Kuhn, M. *caret: Classification and Regression Training*. (2022).
- 1182 75. Meyer, H., Milà, C. & Ludwig, M. *CAST: 'caret' Applications for Spatial-Temporal Models*.
1183 (2022).
- 1184 76. Garbett, S. P. *et al. yaml: Methods to Convert R Data to YAML and Back*. (2022).
- 1185 77. Ushey, K., Allaire, J. J. & Tang, Y. *reticulate: Interface to 'Python'*. (2022).
- 1186 78. Chen, T. *et al. xgboost: Extreme Gradient Boosting*. (2022).
- 1187 79. Garnier *et al. viridis - Colorblind-Friendly Color Maps for R*. (2021).
1188 doi:10.5281/zenodo.4679424.
- 1189 80. Pohlert, T. *trend: Non-Parametric Trend Tests and Change-Point Detection*. (2020).
- 1190 81. Wei, R. & Wang, J. *multiROC: Calculating and Visualizing ROC and PR Curves Across*
1191 *Multi-Class Classifications*. (2018).
- 1192 82. Kassambara, A. *ggpubr: 'ggplot2' Based Publication Ready Plots*. (2020).
- 1193 83. Greenwell, B. *fastshap: Fast Approximate Shapley Values*. (2021).
- 1194 84. Becker, O. S. code by R. A., Minka, A. R. W. R. version by R. B. E. by T. P. & Deckmyn, A.
1195 *maps: Draw Geographical Maps*. (2021).
- 1196 85. Wilke, C. O. & Wiernik, B. M. *ggtext: Improved Text Rendering Support for 'ggplot2'*. (2022).
- 1197 86. Pedersen, T. L. *ggforce: Accelerating 'ggplot2'*. (2022).
- 1198 87. Landau, W. M. The targets R package: a dynamic Make-like function-oriented pipeline
1199 toolkit for reproducibility and high-performance computing. *Journal of Open Source Software*
1200 **6**, 2959 (2021).

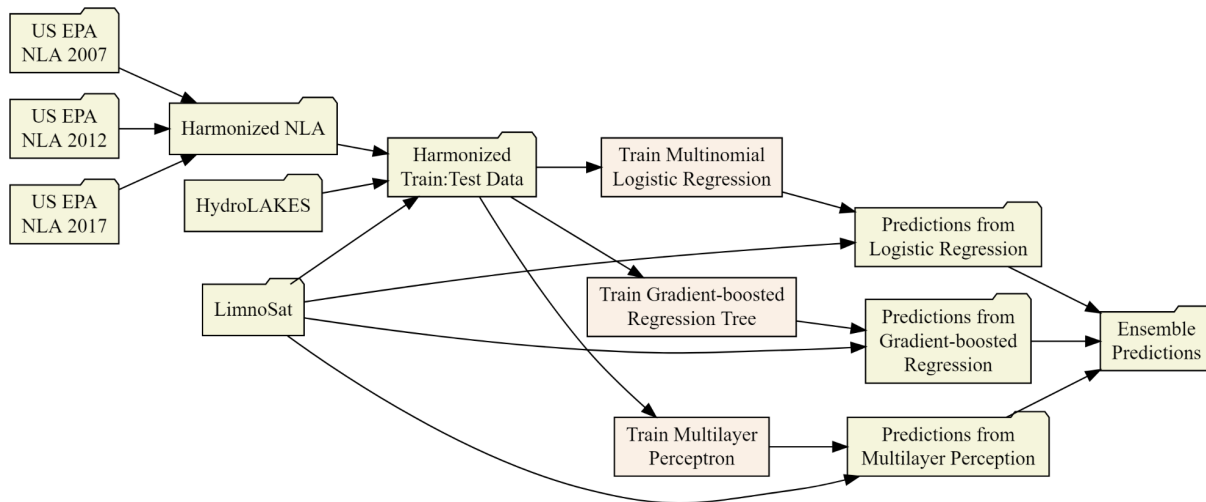
- 1201 88. Oleksy, I. A., Jones, S. E. & Solomon, C. T. Hydrologic Setting Dictates the Sensitivity of
1202 Ecosystem Metabolism to Climate Variability in Lakes. *Ecosystems* (2021)
1203 doi:10.1007/s10021-021-00718-5.
- 1204 89. Iannone, R. *DiagrammeR: Graph/Network Visualization*. (2022).
- 1205
1206



1207
 1208
 1209
 1210
 1211
 1212
 1213
 1214
 1215
 1216
 1217
 1218
 1219
 1220
 1221
 1222
 1223
 1224

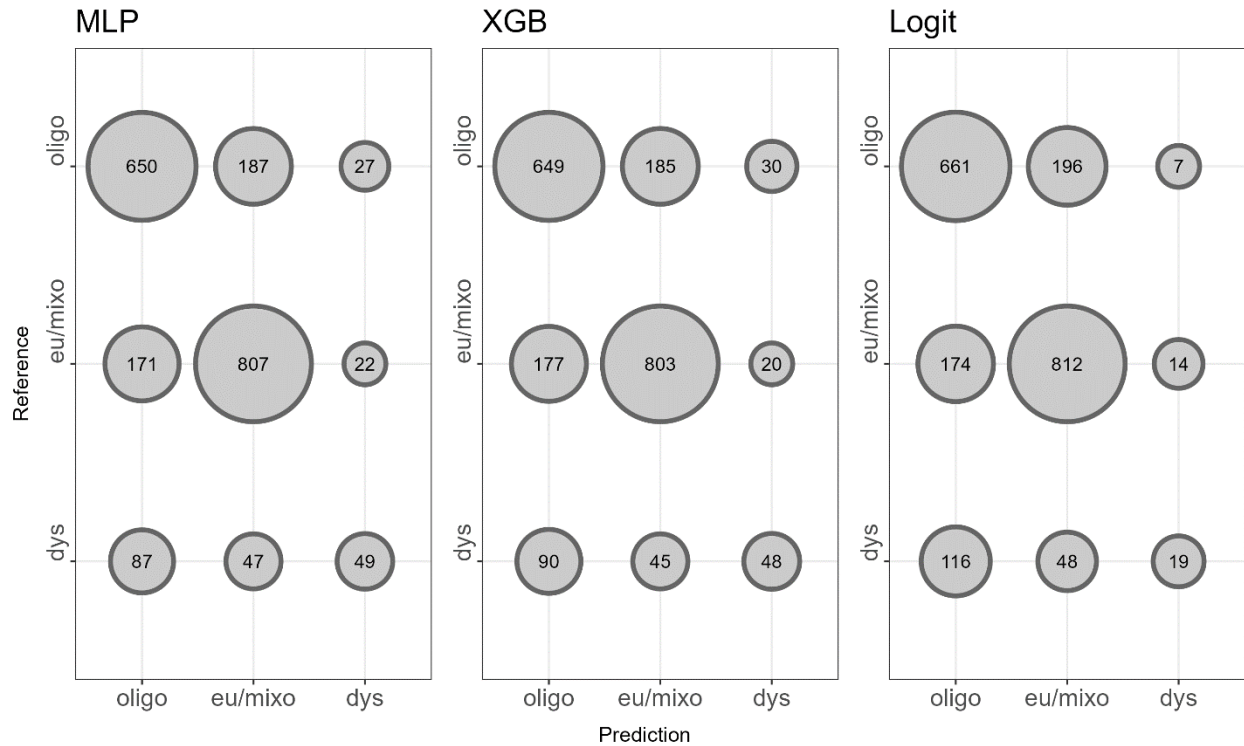
Figure 1: Nutrient-Color Paradigm (NCP) scheme for classifying oligotrophic, eutrophic, dystrophic, and mixotrophic lakes. Schematic is adapted from Williamson et al.²¹ and Webster et al.²², and characteristic lake descriptions broadly stem from results presented in Leech et al.²³ and Oleksy et al.⁸⁸ Within each NCP-quadrant, there are a suite of physical, chemical, and biological characteristics that distinguish each type of lake: colored Dissolved Organic Matter (cDOM), primary production, cyanobacterial abundance, and higher order production. Lower cDOM concentrations (blue water drops) are characteristic in oligotrophic and eutrophic lakes. When cDOM is low, light can transmit through the water column more deeply, allowing for primary producers to undergo photosynthesis and zooplankton to consume primary producers (oligotrophic). When nutrients, such as phosphorus, are at higher concentrations and cDOM is low (eutrophic), primary production, cyanobacterial abundance, and higher order production can all increase, resulting in increased biomass. When cDOM concentrations are high (brown water drop) and nutrient concentrations are low (dystrophic), the increased light attenuation can result in decreased primary production, which can reciprocally cause decreased higher order production. Lastly, when nutrient and cDOM concentrations are

1225 both high (mixotrophic), primary production, cyanobacterial abundance, and higher
1226 order production can exceed values observed when solely cDOM or nutrient
1227 concentrations alone are higher. Phytoplankton and filled-in zooplankton cartoons were
1228 downloaded from the University of Maryland Center for Environmental Science
1229 Integration and Application Network (<https://ian.umces.edu/media-library/>).
1230 Phytoplankton were designed by Tracey Saxby of the Integration and Application
1231 Network, Dieter Tracey of the Water and Rivers Commission, Kim Kraeer and Lucy Van
1232 Essen-Fishman of the Integration and Application Network. Transparent crustacean
1233 zooplankton and rotifer cartoons were drawn by Stephanie E. Hampton.



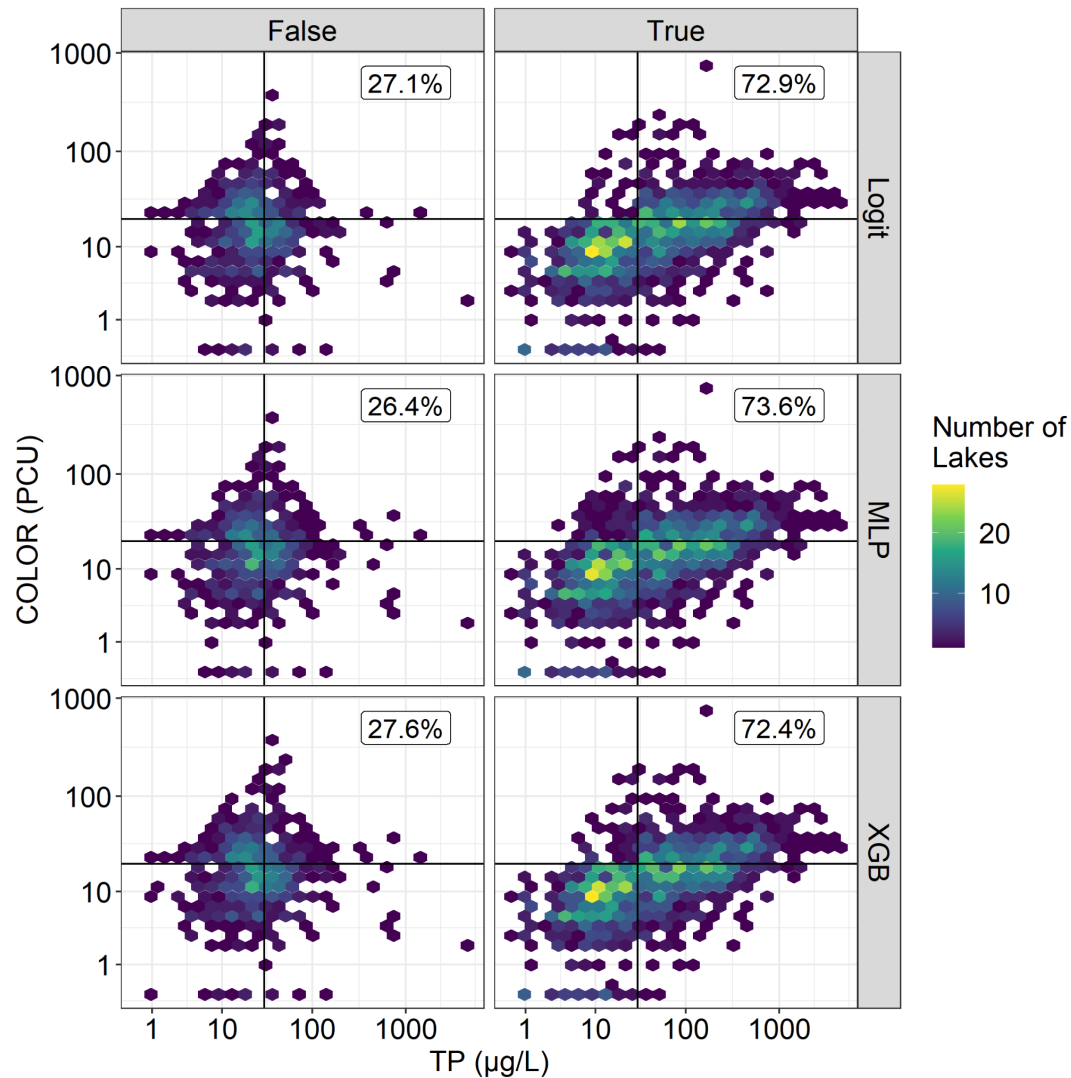
1234
 1235
 1236
 1237
 1238
 1239
 1240
 1241
 1242
 1243
 1244
 1245
 1246
 1247
 1248
 1249
 1250
 1251

Figure 2: Flowchart for data harmonization, modeling, and prediction steps of the LTS-US dataset pipeline. Steps shaped as a file-folder correspond to an intermediary data product, and rectangles correspond to an intermediary model. Data aggregation combines data from the U.S. EPA’s National Lakes Assessment, HydroLAKES, and LimnoSat-US to create a single, harmonized dataset of *in situ* lake trophic states with paired remotely sensed surface reflectances. Model training steps create multinomial logistic regression, multilayer perceptron, and extreme gradient boosted regression tree models. Each fitted model is then applied to the entire LimnoSat-US data, where national-scale predictions are made for each modeling method. Probabilistic predictions are then averaged to create ensemble predictions of lake trophic state. Quality control steps (described in “Technical Validation”) use both the ensemble and individual model predictions to assess model performance. Each of these four components correspond to a piece of the overall data production pipeline: data aggregation functions are described in “1_aggregate”; model training functions are described in “2_train”; national-scale prediction functions are described in “3_predict”; quality control procedures are described in “4_qc”. Flowchart was designed with the “DiagrammeR” package⁸⁹.

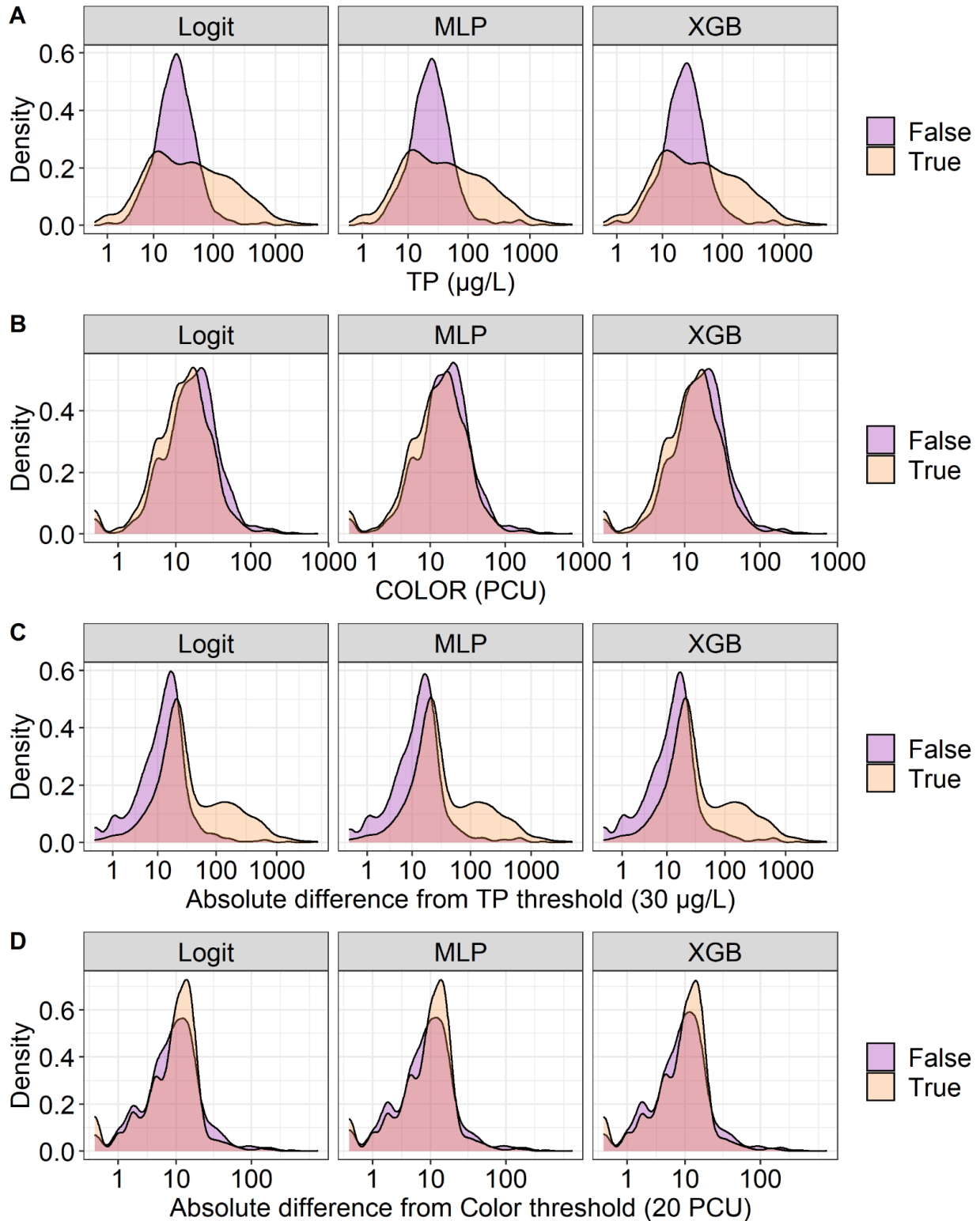


1252
 1253
 1254
 1255
 1256
 1257
 1258
 1259
 1260

Figure 3: Confusion matrices from each modeling approach. Confusion matrices were generated using the test partitions for each spatial-holdout cross-validation. Circle size is scaled by the number of lakes falling within each category. Trophic states for model predictions and reference data correspond to the acronyms “dys” for “dystrophic”, “eu/mixo” for “eutrophic/mixotrophic”, and “oligo” for “oligotrophic”. Model acronyms are located as the title for each confusion matrix, where “MLP” signifies “Multilayer Perceptron”, “XGB” signifies “Gradient Boosted Regression”, and “Logit” signifies “Multinomial Logistic Regression”.



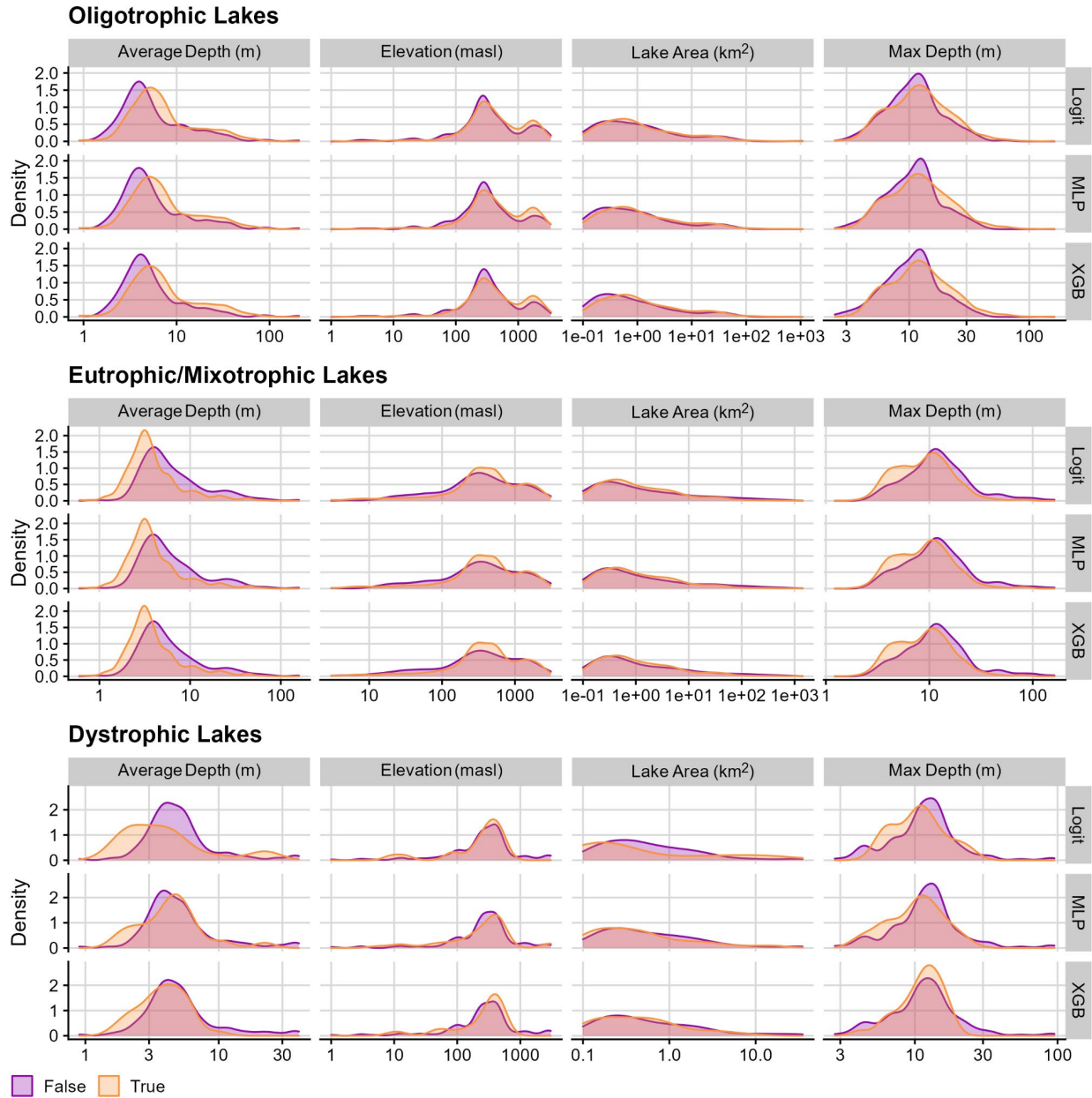
1261
 1262 Figure 4: True and false classifications from testing data displayed on the NCP axes.
 1263 Hexbins are colored by the number of lakes they contain. Labels reflect the percentage
 1264 of lakes correctly or incorrectly predicted within a given modeling technique. Incorrect
 1265 LTS predictions tend to be located at the nexus trophic state groupings. Correct
 1266 predictions tend to more accurately reflect the breadth of ranges that can be observed
 1267 within each of the LTS groupings.



1268
1269
1270
1271
1272

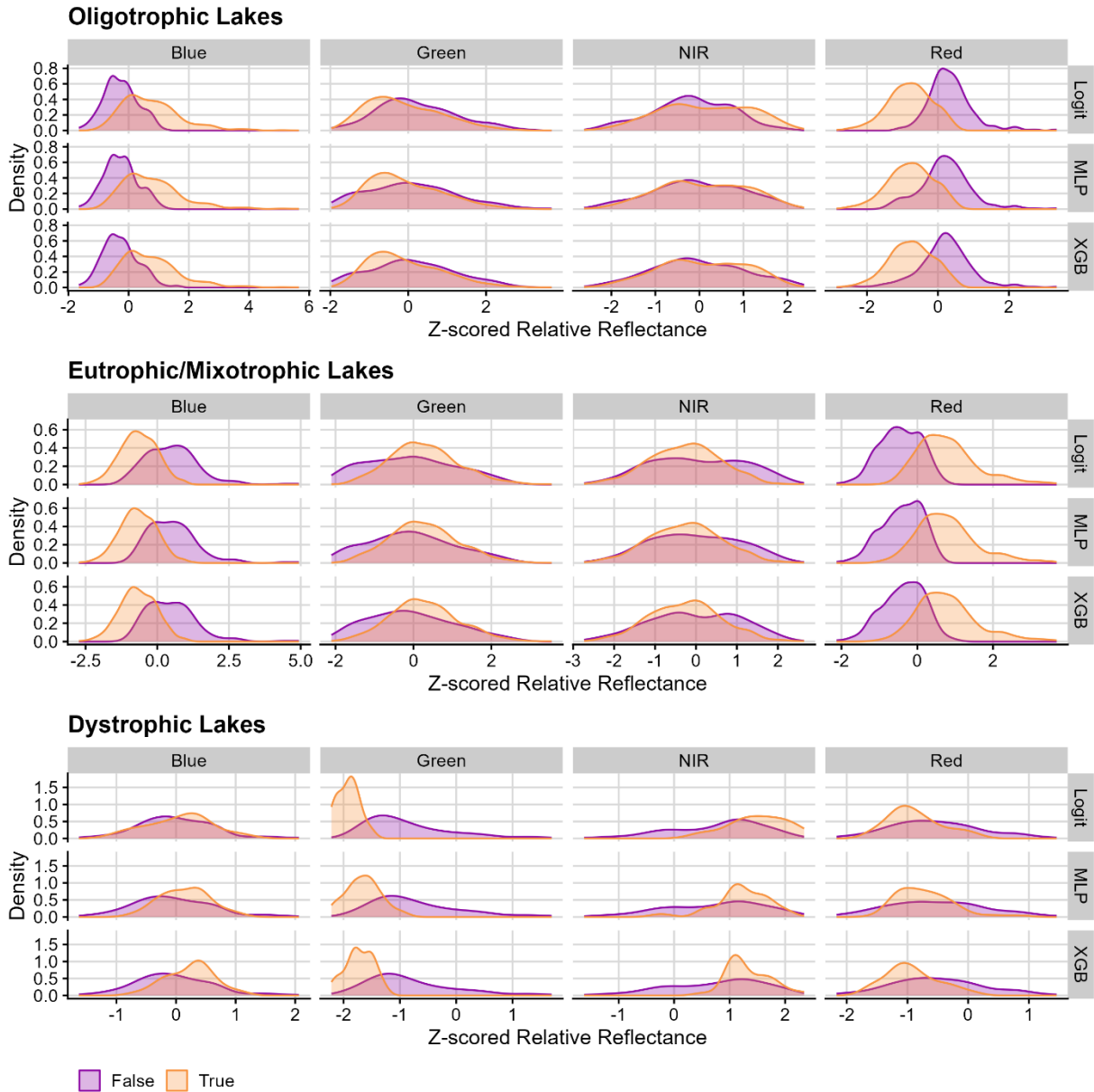
Figure 5: Density plots for total phosphorus (A) and true color (B) values as well as absolute differences from NCP thresholds for total phosphorus (C) and true color (D) among correctly (i.e., True; orange) and incorrectly (i.e., False; purple) classified trophic states. Because misclassifications appeared to increase in frequency near threshold

1273 values for trophic state classification, we also assessed classification accuracies across
1274 absolute differences for each variable and threshold value. Across all models, we
1275 noticed that misclassifications tended to be highest near NCP thresholds for total
1276 phosphorus and color. Total phosphorus concentrations of 15-45 $\mu\text{g/L}$ tended to be
1277 associated with false classifications. True color concentrations of 11-29 PCU tended to
1278 be associated with a false classification.

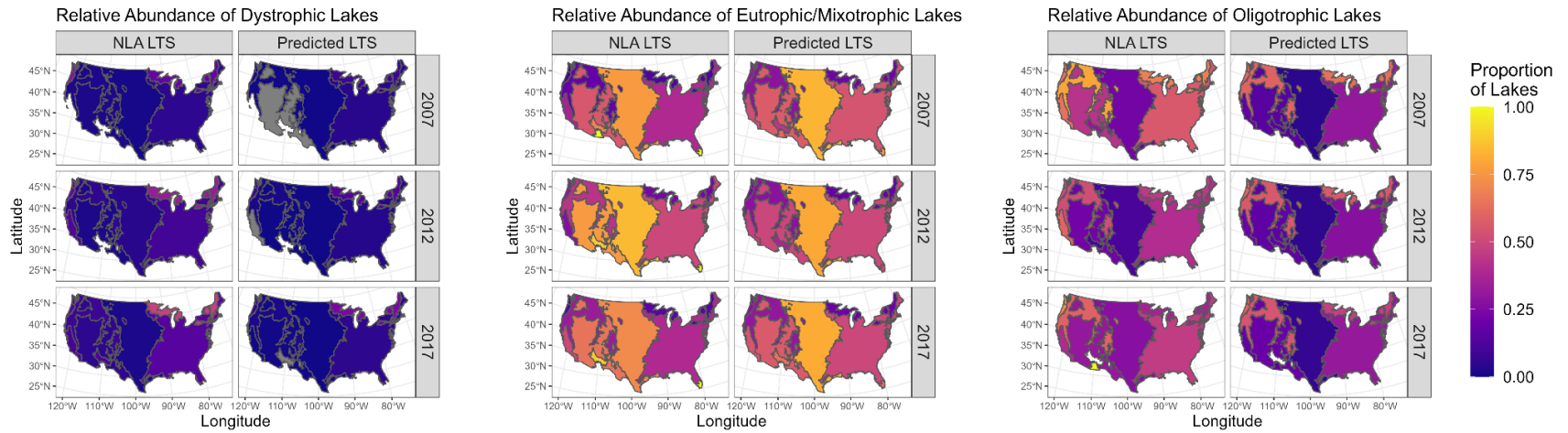


1279
1280
1281
1282
1283
1284
1285
1286
1287

Figure 6: Density distributions for each lake's average depth, elevation, area, and maximum depth values across true (orange) and false (purple) classifications. Values are log-transformed to show characteristic density distributions over a wide range in value magnitudes. In general, patterns across true and false classifications were consistent across all three types of models. Depth was the primary morphometric characteristic for misclassified oligotrophic and eutrophic/mixotrophic lakes, where shallower oligotrophic and deeper eutrophic/mixotrophic lakes tended to be misclassified.



1288
 1289 Figure 7: Density distributions for each Landsat band's z-scored, relative reflectance
 1290 value across true (orange) and false (purple) classifications. In general, patterns across
 1291 true and false classifications were consistent across all three types of models.
 1292 Oligotrophic lakes tended to be misclassified when red bands were high and blue bands
 1293 were low. Conversely, eutrophic/mixotrophic lakes tended to be misclassified when blue
 1294 bands were high, and red bands were low. Dystrophic lakes tended to be misclassified
 1295 when near infra-red bands were low and when green bands were high.



1296
 1297
 1298
 1299

Figure 8: National-scale maps of U.S. Environmental Protection Agency Level I Ecoregions colored by proportion of lakes occurring in that ecoregion. For each trophic state, we compare estimated trophic state relative abundance from the NLA with predicted proportions from the ensemble LTS-US dataset.

Table 1: ANOVA table for total phosphorus and true color measurements in response to model type, model correctness, and trophic state. ANOVAs were assessed with Type II Sum-of-Squares to account for unbalanced sample sizes. To approximate a normal distribution, both total phosphorus and color were log-transformed. A p-value threshold of 0.05 was used to assess significance for each predictor.

(A) Total Phosphorus

	Sum-of-Squares	Degrees of Freedom	F-value	P-value
Model	0	2	0.003	0.997
Correct	5.62	1	43.64	< 0.001
Trophic State	1,335.42	2	5,183.4	< 0.001

(B) Color

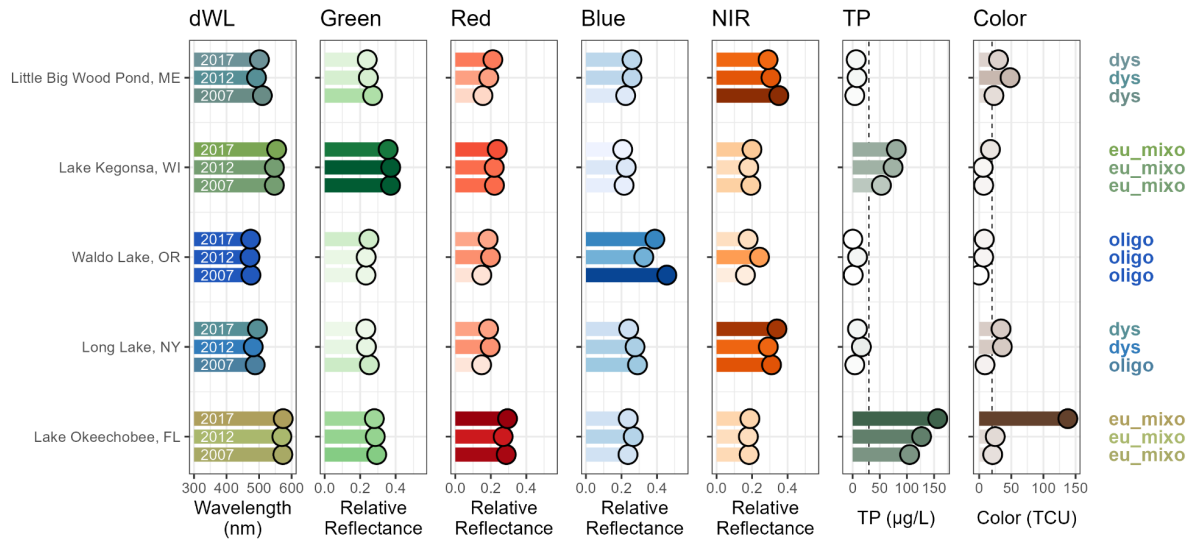
	Sum-of-Squares	Degrees of Freedom	F-value	P-value
Model	0	2	0	1
Correct	0	1	0.02	0.89
Trophic State	286.62	2	1521.80	< 0.001

Table 2: ANOVA table for lake morphological and locational properties in response to model type, model correctness, and trophic state. ANOVAs were assessed with Type II Sum-of-Squares to account for unbalanced sample sizes. To approximate a normal distribution, all response variables were log-transformed. A p-value threshold of 0.05 was used to assess significance for each predictor.

(A) Lake area				
	Sum-of-Squares	Degrees of Freedom	F-value	P-value
Model	0	2	< 0.001	1
Correct	0.4	1	0.76	0.36
Trophic State	35.2	2	33.17	< 0.001
(B) Average Depth				
	Sum-of-Squares	Degrees of Freedom	F-value	P-value
Model	0	2	0.001	1
Correct	1.61	1	14.94	< 0.001
Trophic State	54.32	2	251.53	< 0.001
(C) Maximum Depth				
	Sum-of-Squares	Degrees of Freedom	F-value	P-value
Model	0	2	0.001	1
Correct	1.2	1	16.86	< 0.001
Trophic State	14.17	2	99.53	< 0.001
(D) Elevation				
	Sum-of-Squares	Degrees of Freedom	F-value	P-value
Model	0	2	0.001	1
Correct	3.06	1	10.61	0.001

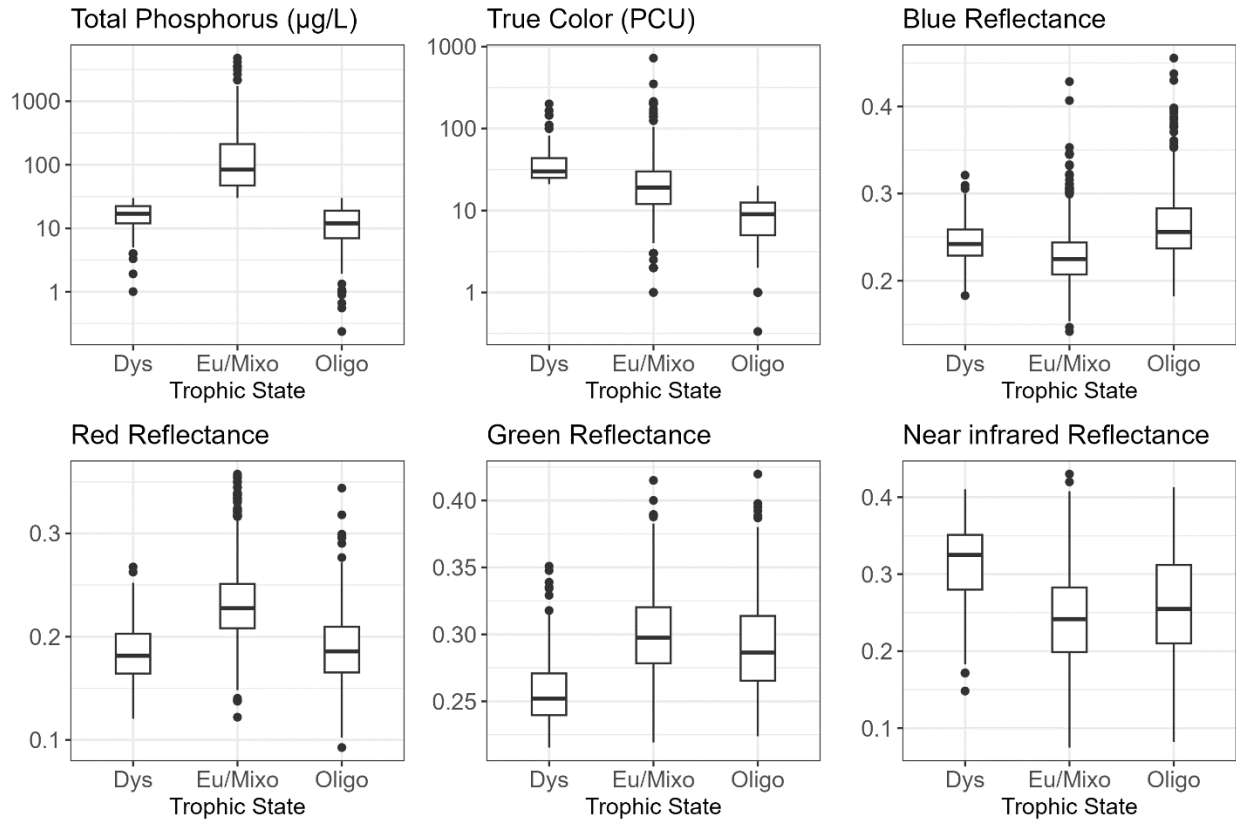
Trophic State	15.39	2	26.63	< 0.001
---------------	-------	---	-------	---------

1303
1304



1305
1306
1307
1308
1309
1310

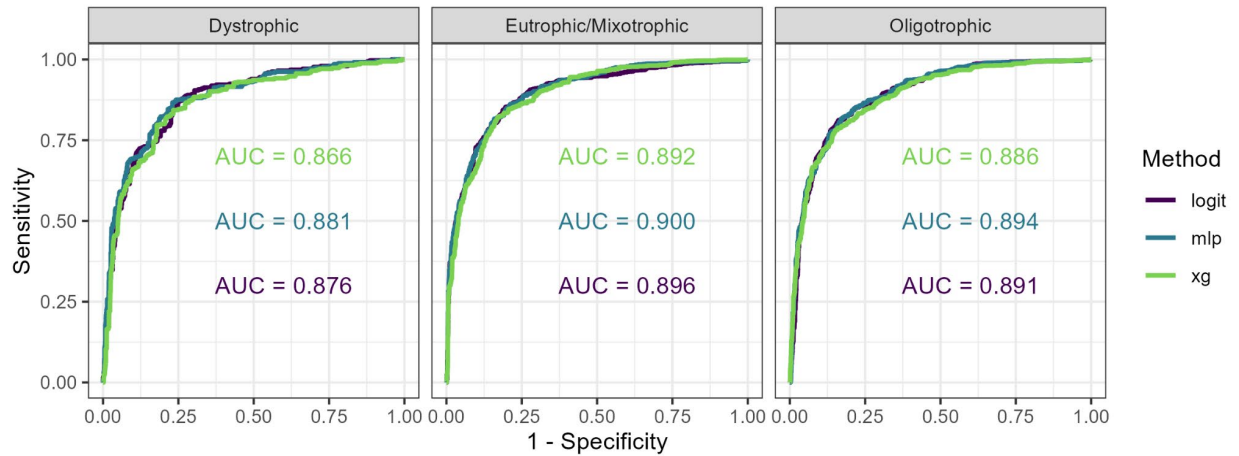
Figure S1: Example comparative summary of five lakes that were sampled in all three U.S. EPA NLA campaigns¹⁻³. In general, variation between lakes is visually greater than within a lake⁴. Colors of a lake's summertime median dominant wavelength (dWL) are represented as the color of the bar and point. All remaining variables are colored by a variable's value, where a darker bar and point refers to a higher variable value.



1311
 1312 Figure S2: Boxplots of all variables used to define trophic state. Total Phosphorus and
 1313 True Color data are shown on a log-scale axis to accommodate multiple orders of
 1314 magnitude.

Table S1: Summary table of training data used for LTS-US Dataset creation¹⁻⁴. These data are used for creating training and test data for each of the three modeling techniques described in the main text. Data are presented as means with standard deviations in parentheses.

Trophic State	Year	Total Phos	Color	Blue	Green	Red	Near Infrared	Number of lakes
Dys	2007	16.05 (6.86)	36.03 (24.12)	0.24 (0.03)	0.26 (0.02)	0.19 (0.03)	0.31 (0.05)	40
Dys	2012	19.36 (7.58)	37.45 (24.21)	0.24 (0.02)	0.26 (0.03)	0.19 (0.04)	0.31 (0.06)	62
Dys	2017	15.78 (6.79)	42.39 (29.96)	0.25 (0.02)	0.26 (0.03)	0.18 (0.02)	0.32 (0.05)	81
Eu/Mixo	2007	233.3 (401.7)	19.87 (14.75)	0.22 (0.03)	0.3 (0.03)	0.23 (0.04)	0.25 (0.06)	362
Eu/Mixo	2012	196.61 (362.4)	26.82 (41.71)	0.23 (0.03)	0.3 (0.03)	0.23 (0.04)	0.24 (0.06)	386
Eu/Mixo	2017	169.01 (332.2)	28.12 (35.53)	0.23 (0.03)	0.3 (0.03)	0.23 (0.03)	0.24 (0.06)	252
Oligo	2007	10.85 (7.45)	8.01 (4.91)	0.26 (0.04)	0.29 (0.03)	0.19 (0.03)	0.26 (0.07)	411
Oligo	2012	16.25 (7.5)	10.89 (4.85)	0.26 (0.04)	0.29 (0.04)	0.18 (0.03)	0.26 (0.07)	229
Oligo	2017	14.01 (6.96)	8.58 (6.03)	0.27 (0.04)	0.29 (0.03)	0.19 (0.03)	0.26 (0.06)	224



1317

1318

1319

1320

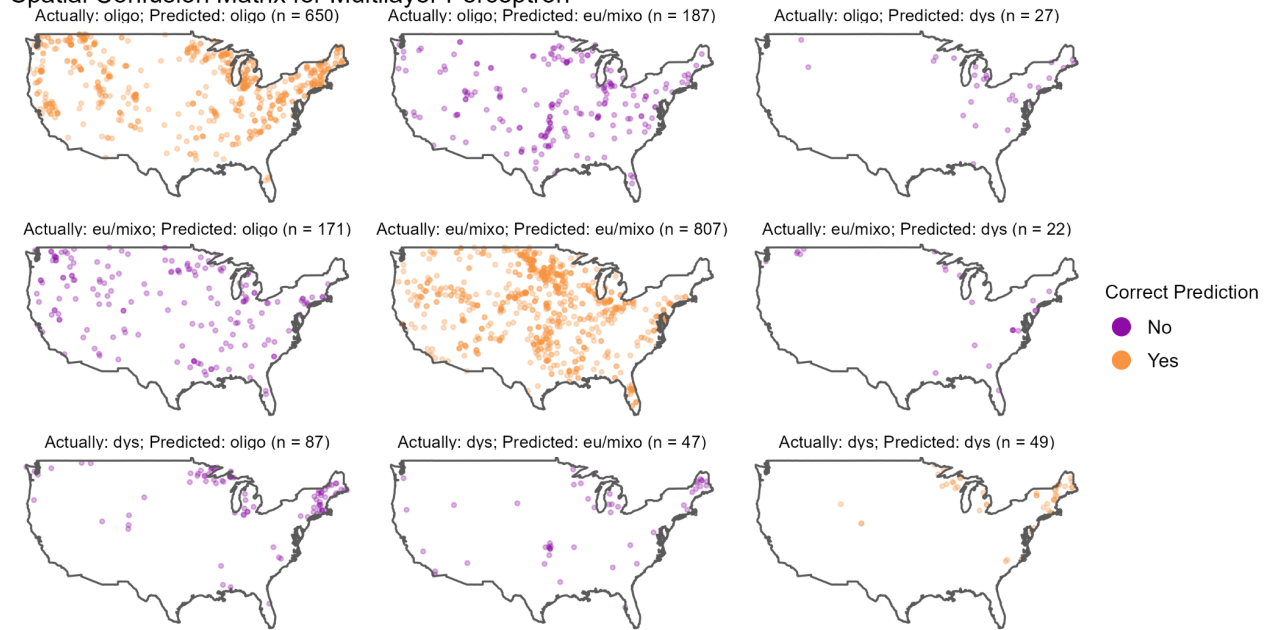
1321

1322

1323

Figure S3: Receiver-Operator-Characteristic (ROC) curves for each trophic status prediction and model method. Area under the Curve (AUC) is reported for each ROC curve. AUC is a metric that generally reflects model fit, where the ROC curve details a model's capacity to give a true result as the false positive rate is artificially inflated. Across all LTS and modeling methods, ROC curves and resulting AUCs are exceptionally similar, suggesting overall congruence among modeling methodologies.

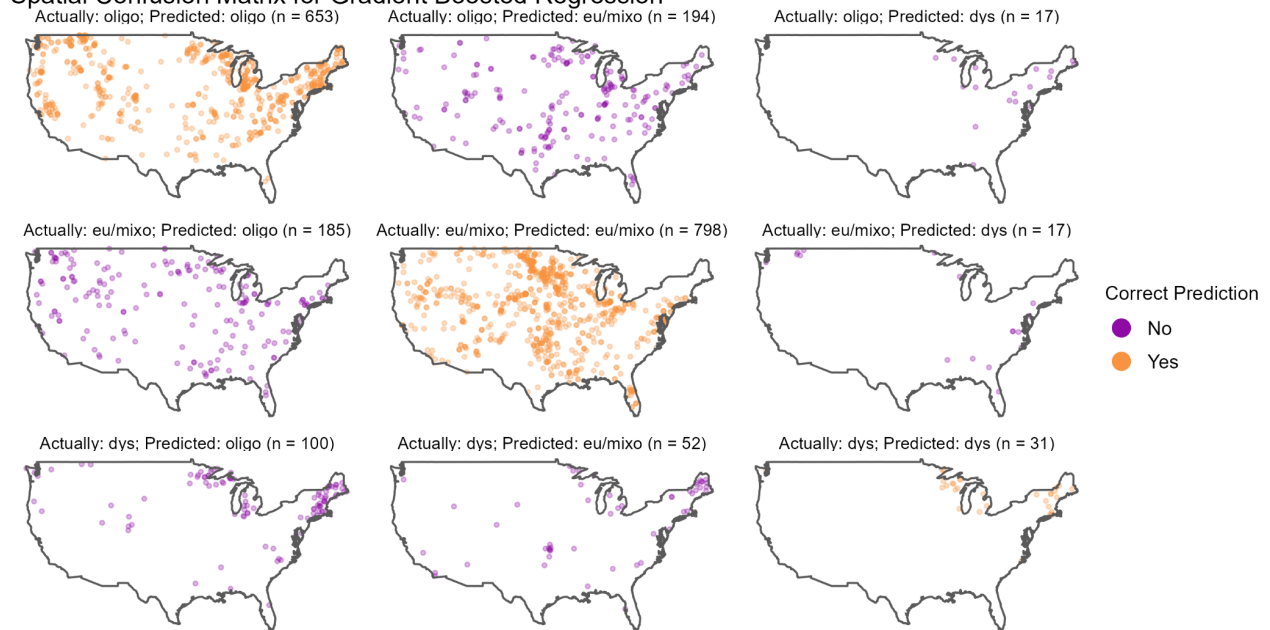
Spatial Confusion Matrix for Multilayer Perceptron



1324
1325
1326
1327
1328

Figure S4: Spatial confusion matrix for multilayer perceptron model. In general, the multilayer perceptron model did not classify or misclassify lakes in a spatial pattern, giving confidence that models were likely misclassifying due to differences other than locational biases at the continental scale.

Spatial Confusion Matrix for Gradient Boosted Regression

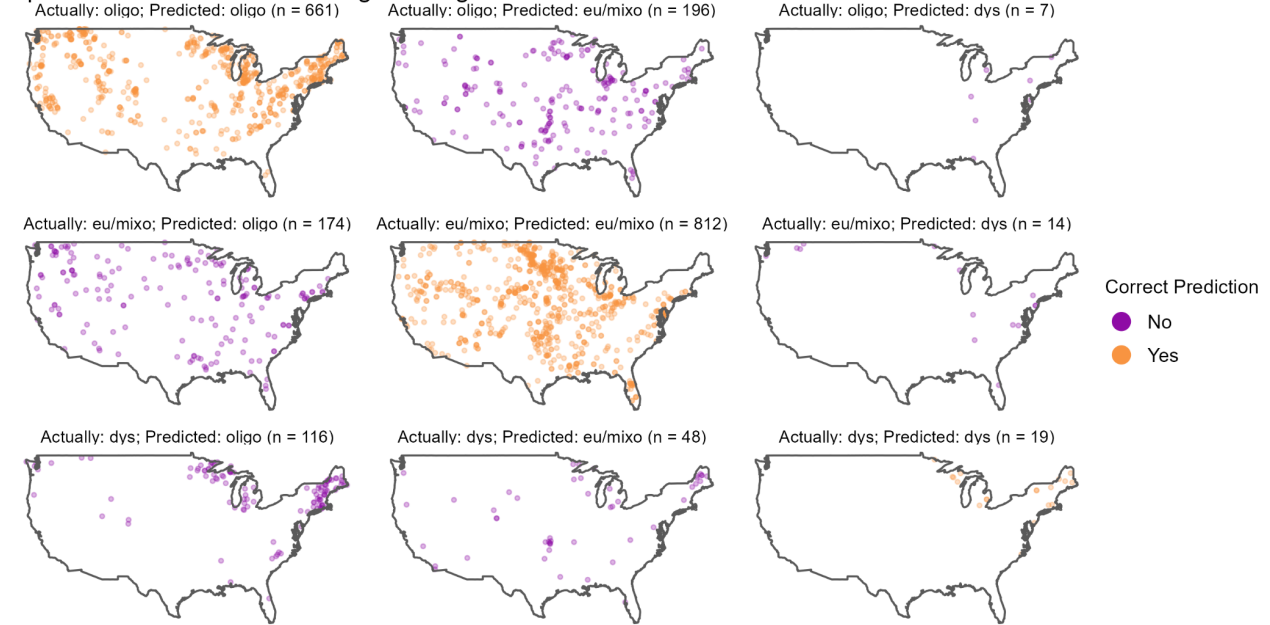


1329
1330
1331
1332
1333

Figure S5: Spatial confusion matrix for gradient boosted regression model. In general, the model did not classify or misclassify lakes in a spatial pattern, giving confidence that models were likely misclassifying due to differences other than locational biases at the continental scale.

1334

Spatial Confusion Matrix for Logistic Regression



1335

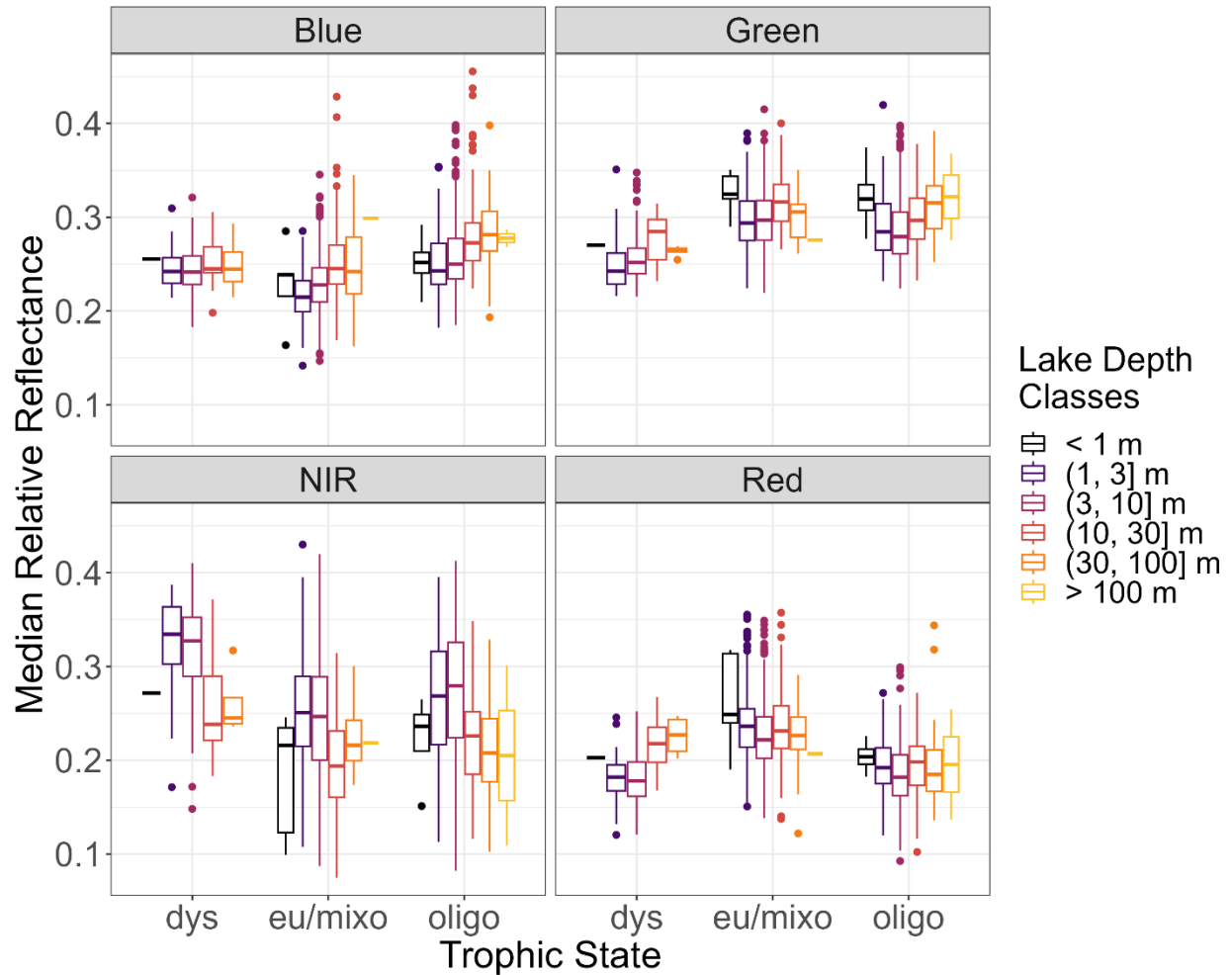
1336

1337

1338

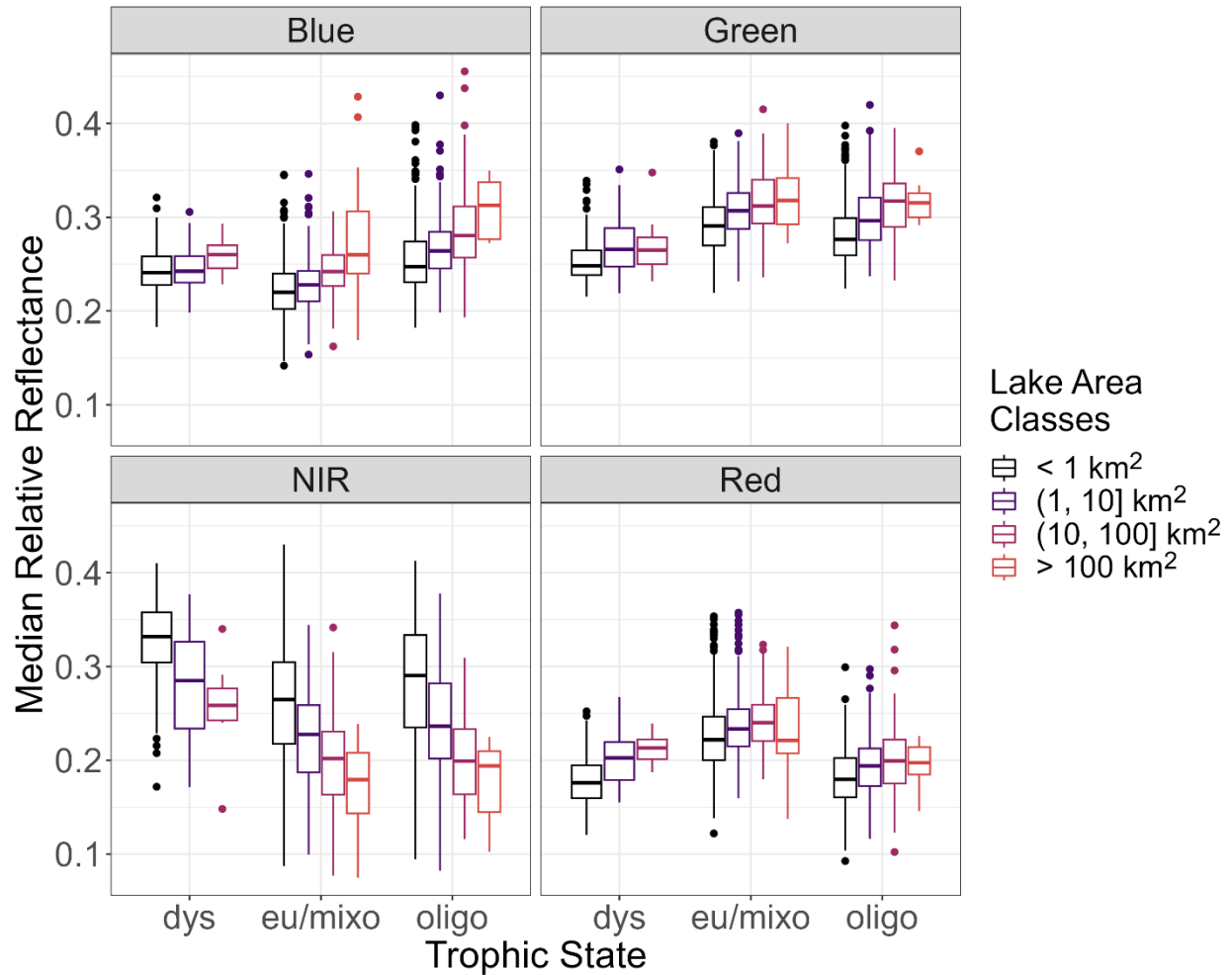
1339

Figure S6: Spatial confusion matrix for Logit model. In general, the Logit model did not classify or misclassify lakes in a spatial pattern, giving confidence that models were likely misclassifying due to differences other than locational biases at the continental scale.



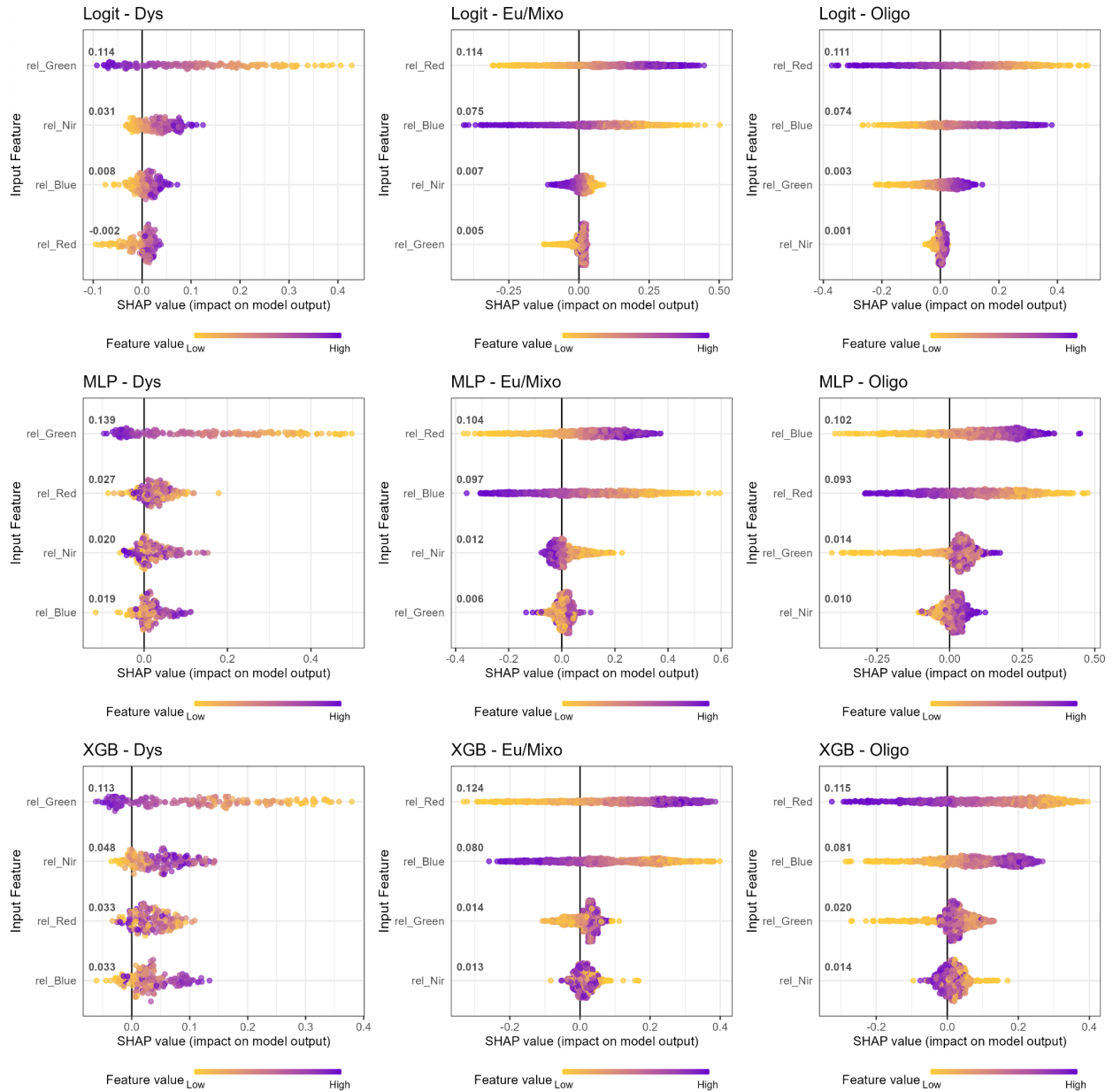
1340
 1341
 1342
 1343
 1344
 1345
 1346
 1347

Figure S7: Boxplots of median summertime relative reflectance values for each Landsat band and NCP-defined trophic state divided by lake depth classes. Water quality data are aggregated from the 2007, 2012, and 2017 U.S. EPA NLA campaigns. Reflectance data are aggregated from LimnoSat-US. Relative reflectance is defined as the value of a given band's reflectance divided by the sum of all four bands. Summertime median relative reflectances are defined as the median of all relative reflectance values from June through August in a given year.



1348
 1349
 1350
 1351
 1352
 1353
 1354
 1355

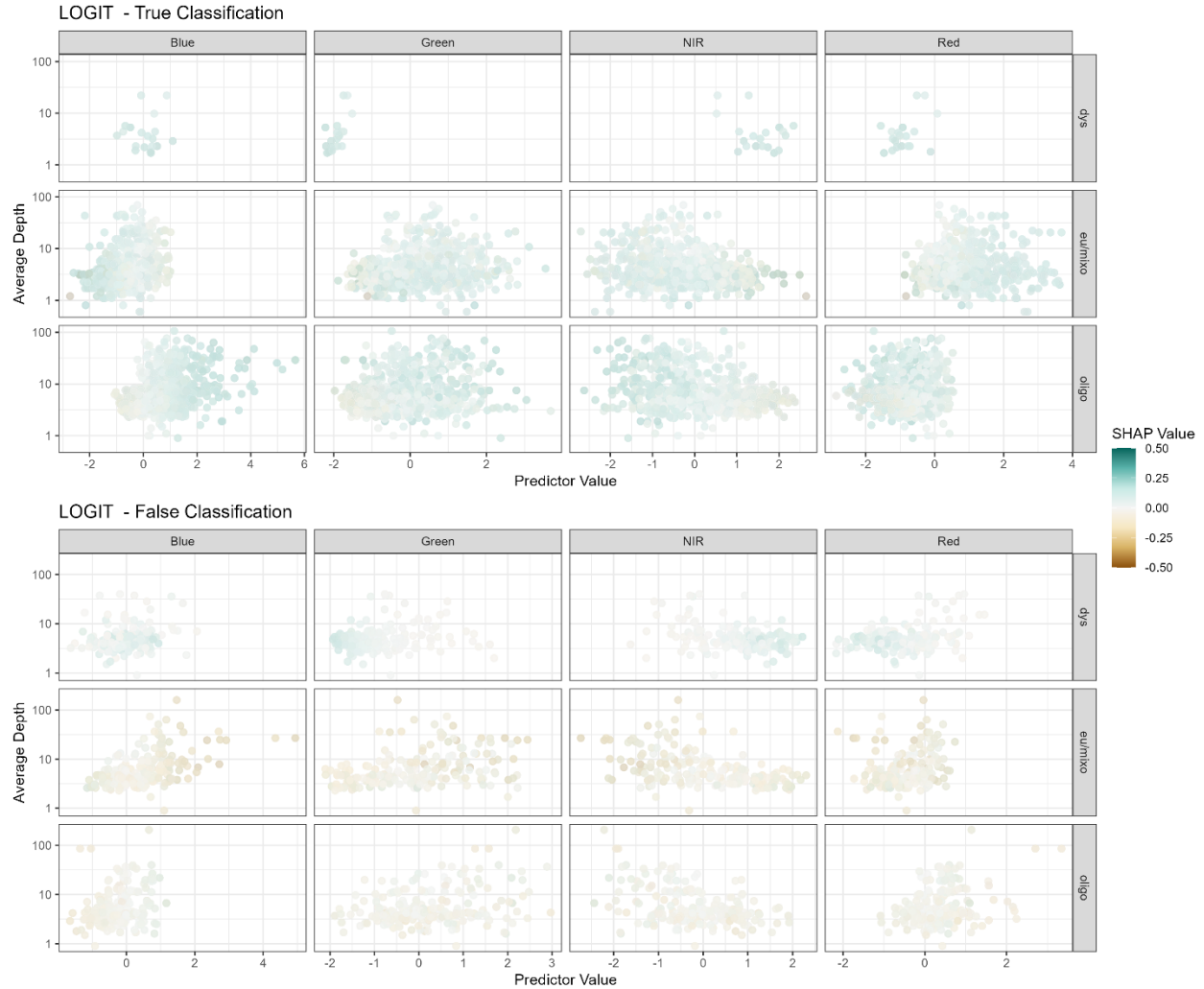
Figure S8: Boxplots of median summertime relative reflectance values for each Landsat band and NCP-defined trophic state divided by lake area classes. Water quality data are aggregated from the 2007, 2012, and 2017 U.S. EPA NLA campaigns. Reflectance data are aggregated from LimnoSat-US. Relative reflectance is defined as the value of a given band's reflectance divided by the sum of all four bands. Summertime median relative reflectances are defined as the median of all relative reflectance values from June through August in a given year.



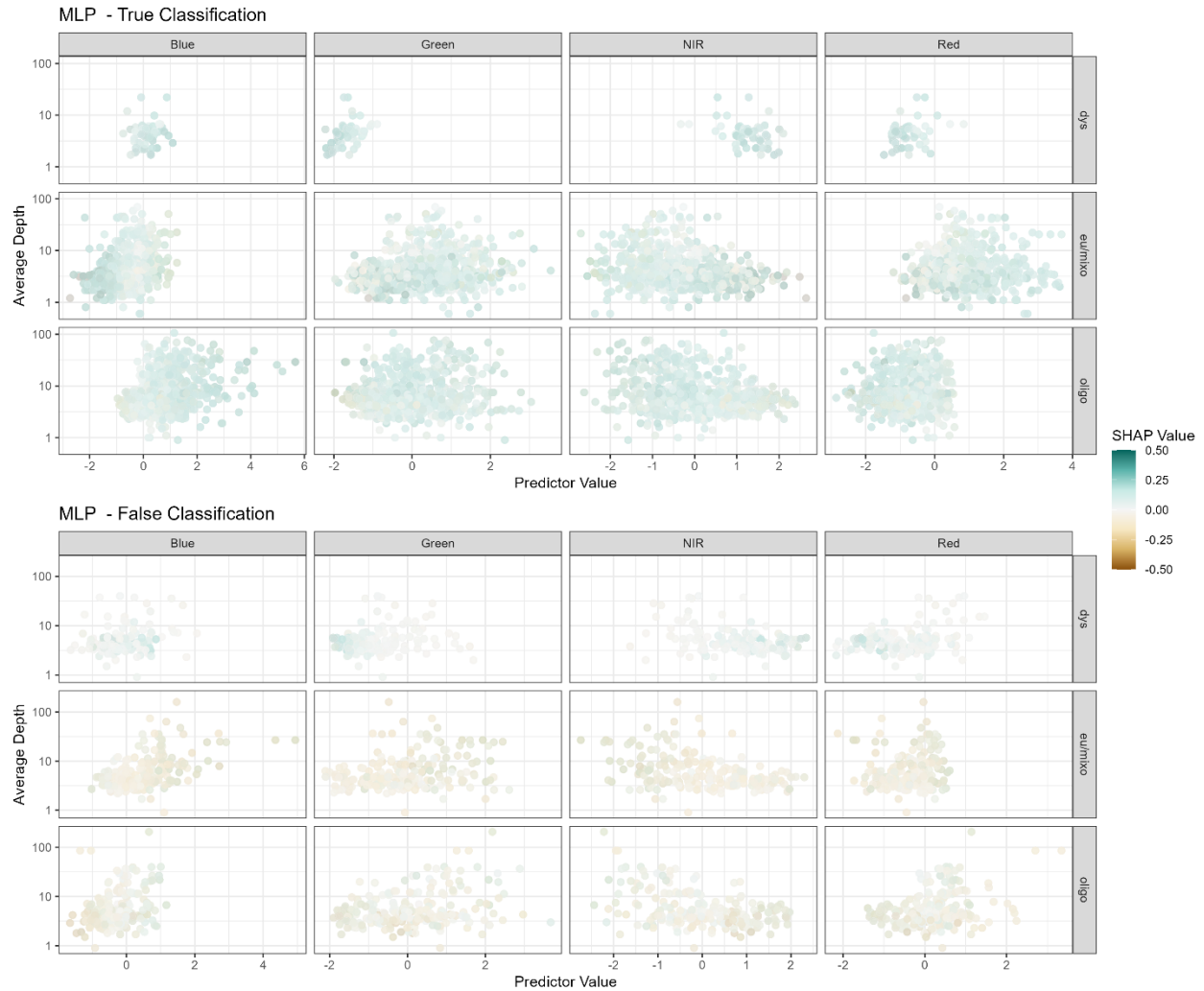
1356
 1357
 1358
 1359
 1360
 1361
 1362
 1363
 1364
 1365
 1366
 1367
 1368

Figure S9: Summary plots from SHAP analysis with SHAP values arranged by model type and lake trophic state. SHAP values include those from correct and incorrect classifications. Importance scores are located next to each feature on the left side of each plot panel. Features are arranged on the y-axis of each plot in order of relative importance, where most important features are at the top of the plot and decrease in relative importance towards the bottom of the plot. Across all modeling types, features were comparable in importance. In all cases, the top two features for each modeling technique and trophic state were identical. Further, the top two features also corresponded to limnological and ecological understanding of each lake type. Dystrophic lakes were most influenced by green and near-infrared bands, which corresponds to these lakes being characterized by increased sediment and dissolved organic carbon as well as decreased primary production. Eutrophic/mixotrophic and

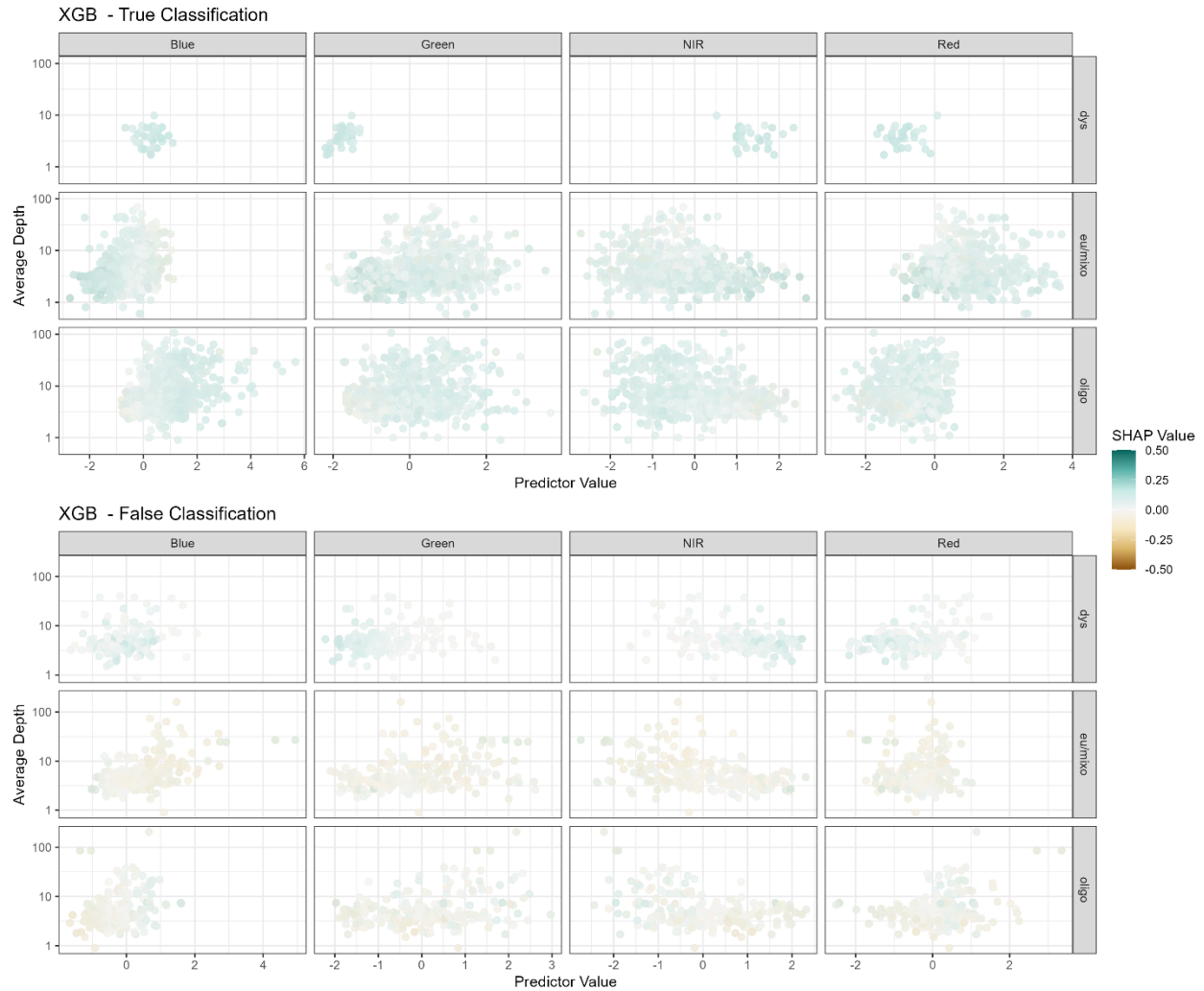
1369 oligotrophic lakes were most influenced by red and blue bands, which corresponds to
1370 these lakes as being most characterized by primary production.



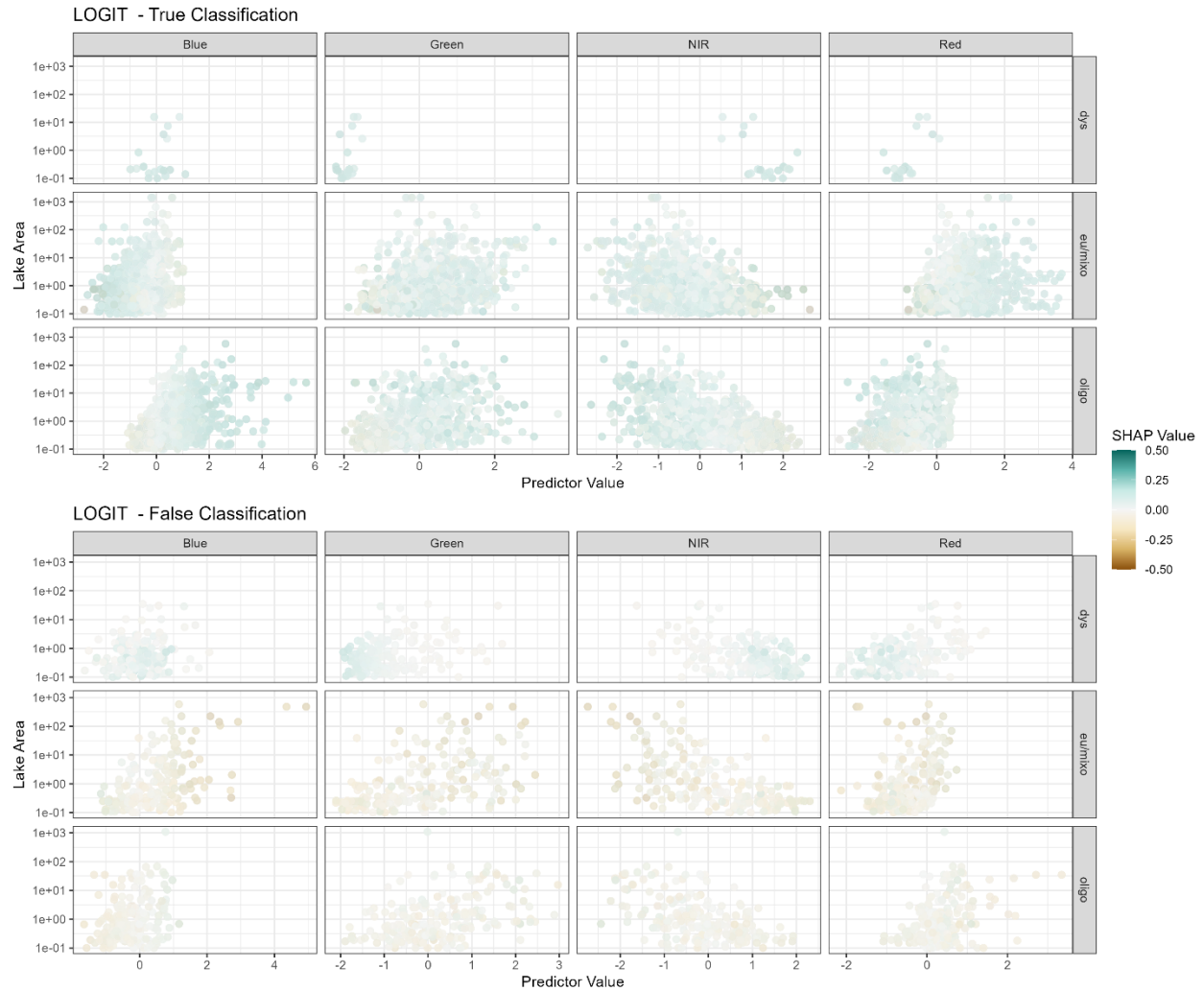
1371
 1372 Figure S10: SHAP value analysis by each trophic state's band value and average depth
 1373 from logistic regression models. While correct and incorrect classifications generally
 1374 occupied the same parameter space for band values and average depths, greatest
 1375 incongruence between correct and incorrect classifications occurred in blue and red
 1376 bands for eutrophic and oligotrophic lakes. In particular, shallow oligotrophic lakes
 1377 tended to have lower blue reflectances, which corresponded to a lower SHAP value;
 1378 shallow eutrophic/mixotrophic lakes likewise had low blue reflectances, but these bands
 1379 had high SHAP values. Conversely, deeper oligotrophic lakes tended to have lower red
 1380 band values, which were associated with higher SHAP values; deeper
 1381 eutrophic/mixotrophic lakes tended to have higher red reflectances, which also had a
 1382 higher SHAP value. Together, this analysis suggests that lakebed effects may influence
 1383 classification. For example, benthic algal production in oligotrophic lakes may produce
 1384 reflectance values similar to eutrophic lakes, leading to model confusion. This same
 1385 result is implied throughout all analysis steps, where depth appears to be the major
 1386 issue for correct trophic state classification.



1387
 1388 Figure S11: SHAP value analysis by each trophic state's band value and average depth
 1389 from multilayer perceptron models. While correct and incorrect classifications generally
 1390 occupied the same parameter space for band values and average depths, greatest
 1391 incongruence between correct and incorrect classifications occurred in blue and red
 1392 bands for eutrophic and oligotrophic lakes. In particular, shallow oligotrophic lakes
 1393 tended to have lower blue reflectances, which corresponded to a lower SHAP value;
 1394 shallow eutrophic/mixotrophic lakes likewise had low blue reflectances, but these bands
 1395 had high SHAP values. Conversely, deeper oligotrophic lakes tended to have lower red
 1396 band values, which were associated with higher SHAP values; deeper
 1397 eutrophic/mixotrophic lakes tended to have higher red reflectances, which also had a
 1398 higher SHAP value. Together, this analysis suggests that lakebed effects may influence
 1399 classification. For example, benthic algal production in oligotrophic lakes may produce
 1400 reflectance values similar to eutrophic lakes, leading to model confusion.

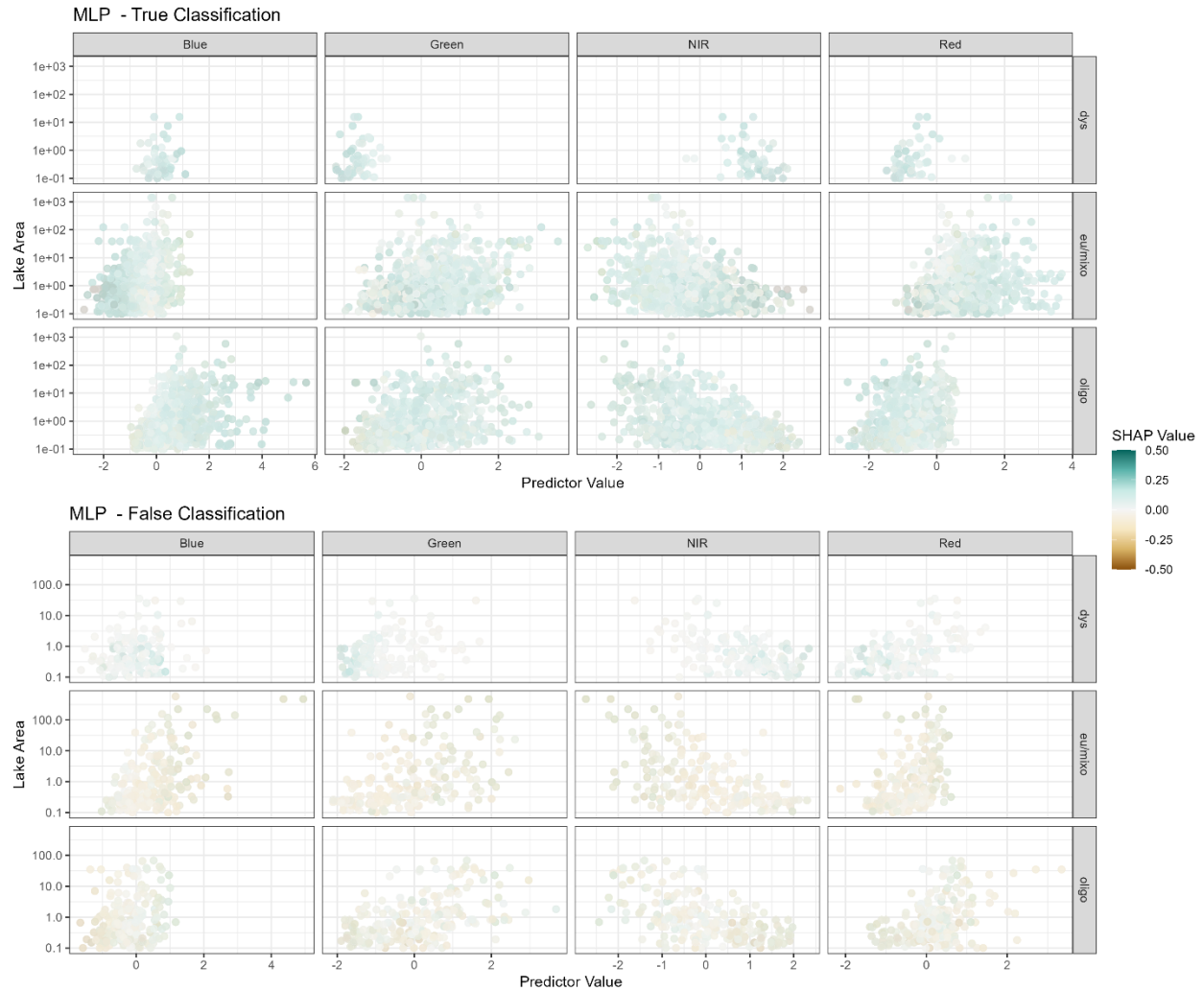


1401
 1402 Figure S12: SHAP value analysis by each trophic state's band value and average depth
 1403 from gradient boosted regression models. While correct and incorrect classifications
 1404 generally occupied the same parameter space for band values and average depths,
 1405 greatest incongruence between correct and incorrect classifications occurred in blue
 1406 and red bands for eutrophic and oligotrophic lakes. In particular, shallow oligotrophic
 1407 lakes tended to have lower blue reflectances, which corresponded to a lower SHAP
 1408 value; shallow eutrophic/mixotrophic lakes likewise had low blue reflectances, but these
 1409 bands had high SHAP values. Conversely, deeper oligotrophic lakes tended to have
 1410 lower red band values, which were associated with higher SHAP values; deeper
 1411 eutrophic/mixotrophic lakes tended to have higher red reflectances, which also had a
 1412 higher SHAP value. Together, this analysis suggests that lakebed effects may influence
 1413 classification. For example, benthic algal production in oligotrophic lakes may produce
 1414 reflectance values similar to eutrophic lakes, leading to model confusion.



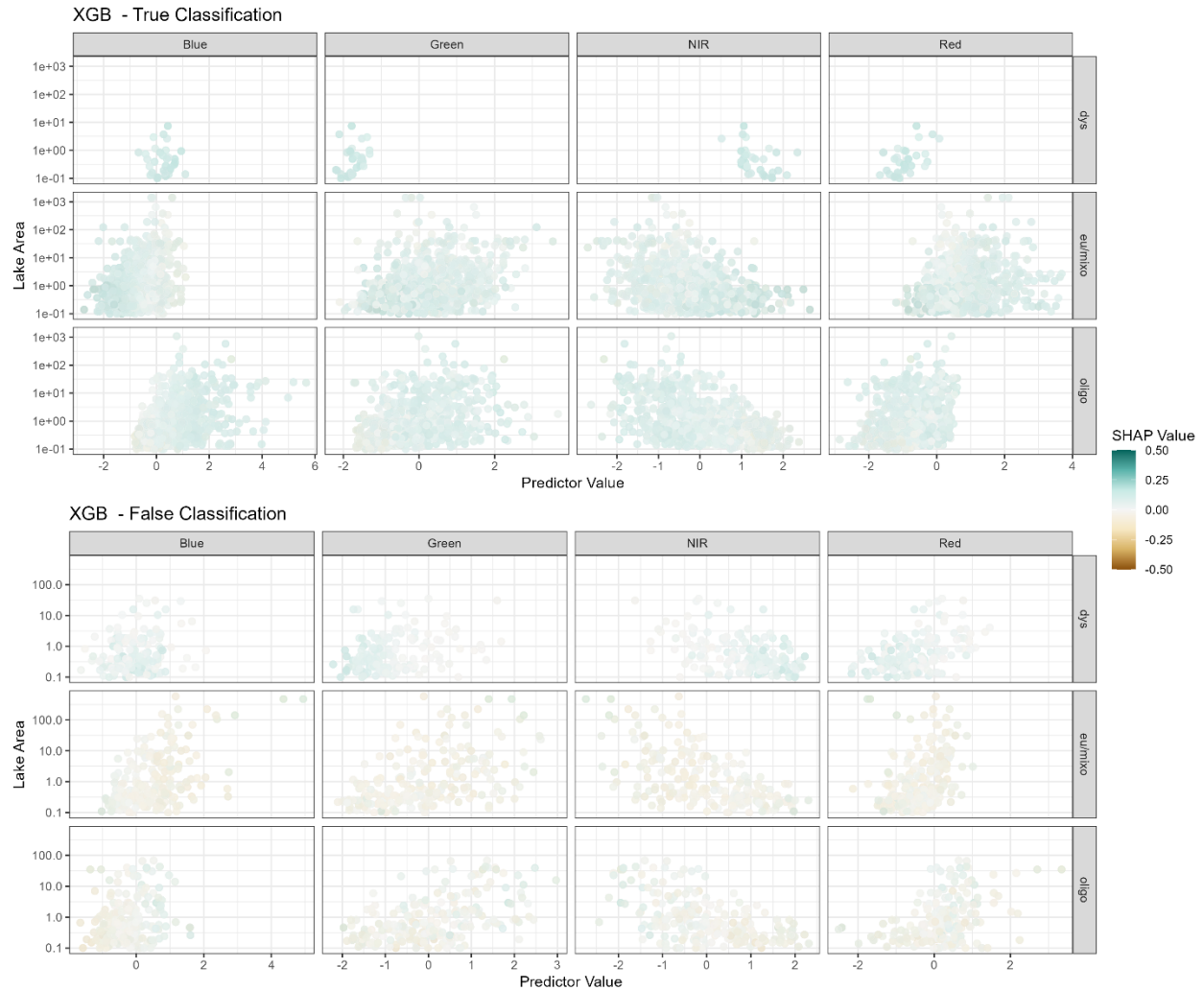
1415
 1416
 1417
 1418
 1419
 1420
 1421

Figure S13: SHAP value analysis by each trophic state's band value and surface area from logistic regression models. Visually, SHAP and reflectance values as well as lake areas all occupied the same parameter space, implying that lake area, a proxy for adjacency effects, is likely not consequential for feature importance and correct classification. This general result is likewise observed in lake areas being generally consistent across correctly and incorrectly classified lakes.



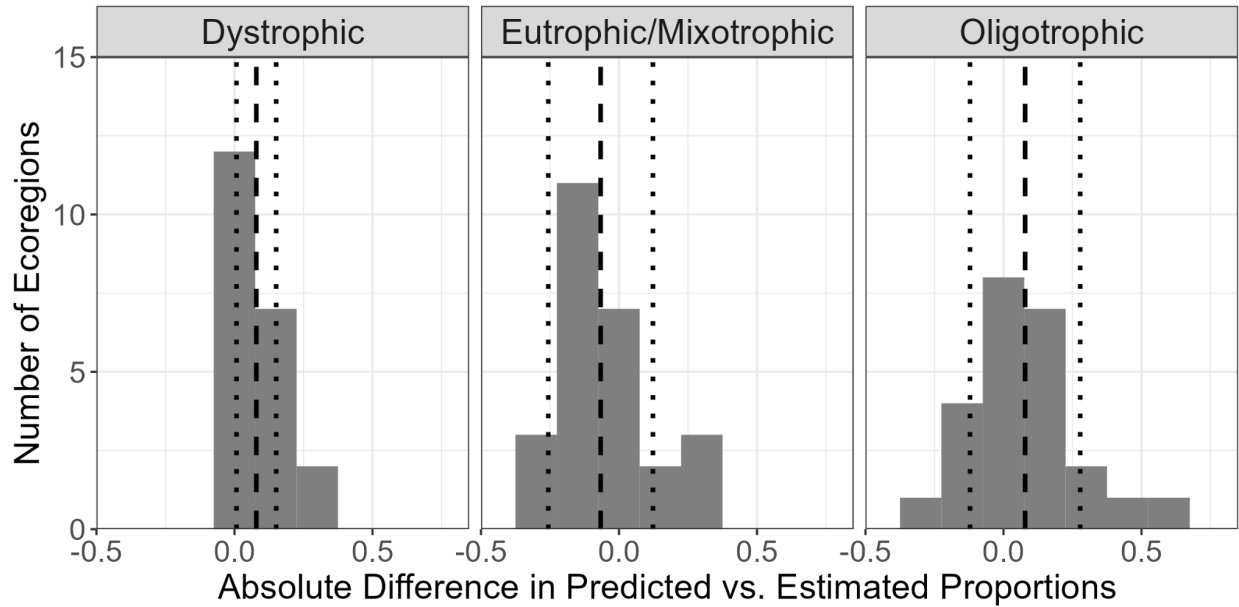
1422
 1423
 1424
 1425
 1426
 1427
 1428

Figure S14: SHAP value analysis by each trophic state's band value and surface area from multilayer perceptron models. Visually, SHAP and reflectance values as well as lake areas all occupied the same parameter space, implying that lake area, a proxy for adjacency effects, is likely not consequential for feature importance and correct classification. This general result is likewise observed in lake areas being generally consistent across correctly and incorrectly classified lakes.



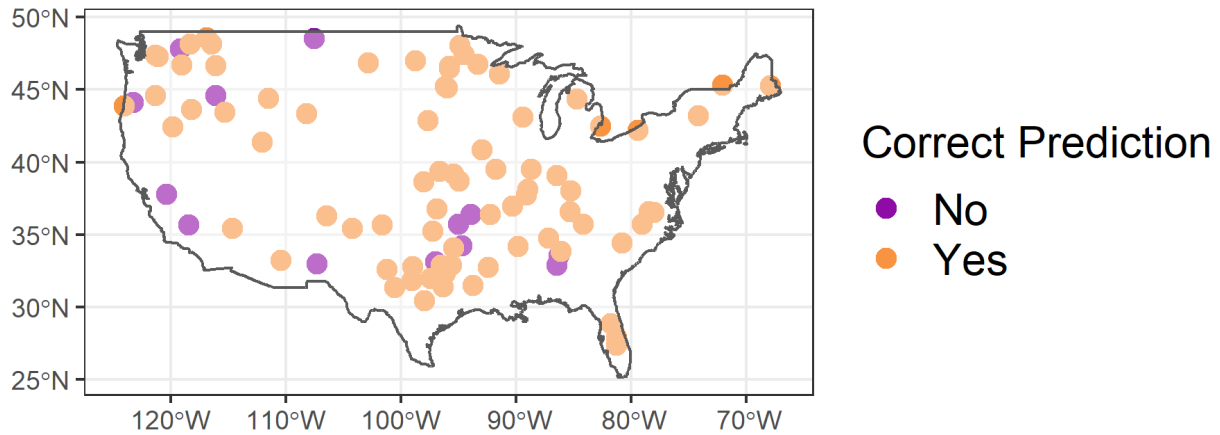
1429
 1430
 1431
 1432
 1433
 1434
 1435

Figure S15: SHAP value analysis by each trophic state's band value and surface area from gradient boosted regression models. Visually, SHAP and reflectance values as well as lake areas all occupied the same parameter space, implying that lake area, a proxy for adjacency effects, is likely not consequential for feature importance and correct classification. This general result is likewise observed in lake areas being generally consistent across correctly and incorrectly classified lakes.



1436
 1437
 1438
 1439
 1440
 1441
 1442

Figure S16: Histograms of absolute difference (Estimated - Predicted) in predicted and estimated proportions of each lake trophic state across U.S. EPA Level I Ecoregions. Vertical dashed lines reflect the mean, and vertical, dotted lines reflect one standard deviation from the mean. For all trophic states, distributions approximately center around zero. Oligotrophic and dystrophic lakes tend to be slightly underpredicted, whereas eutrophic and mixotrophic lakes tend to be slightly overpredicted.



1443
 1444
 1445
 1446
 1447
 1448
 1449
 1450
 1451

Figure S17: National-scale map of correct and incorrect trophic state classifications as assessed by manual checking of lake trophic state predictions against independent sources. Among lakes where independent sources could be identified, 73.5% of lakes were correctly predicted, which is notably similar to accuracies assessed from the NLA sampling campaign data. Additionally, correct and incorrect classifications did not follow apparent spatial patterns, implying that our models were not influenced by geographical or locational differences.